Master Thesis

On the Development of a Volumetric Acoustic Emission Fatigue Crack Monitoring System

B. Scheeren

24 October 2017

TU Delft

vallen systeme

Master Thesis

On the Development of a Volumetric Acoustic Emission Fatigue Crack Monitoring System

by

B. Scheeren

To obtain the Degree of Master of Science

Delft University of Technology
Faculty of Mechanical, Maritime & Materials Engineering
Department of Maritime & Transport Technology
Section of Ship Hydromechanics & Structures

&

Vallen Systeme GmbH

Student number:	4151941	
Supervisors:	Prof. dr. ir. M.L. Kaminski,	TU Delft, supervisor
	Dr. T. Thenikl,	Vallen Systeme, supervisor
	D. Altmann B.Sc. Math,	Vallen Systeme, supervisor
Date of Defence:	30 October 2017	
Assessment Committee:	Prof. dr. ir. M.L. Kaminski,	TU Delft, Chair
	Ir. P.S. van Lieshout,	TU Delft
	Dr. ir. P.Th.L.M. van Woerkom,	TU Delft
	Dr. ir. M. Janssen,	TU Delft
	Dr. T. Thenikl,	Vallen Systeme

An electronic version of this document is available at https://repository.tudelft.nl/.

TU Delft Delft University of Technology

vallen systeme

πάντα ῥεῖ
everything flows

Heraclitus of Ephesus

Preface

Everything flows are two words that have allegedly been spoken by Heraclitus of Ephesus; be it not in modern English but rather ancient Greek or a local Persian dialect. They characterise the persistent change that the world is subjected to. In this sense these words are particularly suited to describe contents of this document.

The project contained within this thesis aspired to observe the changes in a specimen when it is subjected to cyclic loading. However, when the specimen did not show any changes, it was required that the project would be changed. Change is inevitable. The crux is how one manages to adapt to it.

Just how well I dealt with this change may be concluded from the research I present to you through this document. My thesis has been finalised, and the past year of doing so has been dynamic and most certainly a grand experience. Though at certain times progress seemed to halt, and this made it difficult to always keep up the positive spirit. In these times support could be drawn from Marcus Aurelius' *Meditations*. Which freely paraphrased state that hardship is no sign of impossibility, and whatsoever may be possible, I can do.

Besides the wisdom of the old philosophers there are some people to be thankful for. Of course Mirek for his everlasting fate in my competence, especially in those times I was doubting the progress we made. Daniel, Thomas, Hans-Peter and Thomas, and the other colleagues at Vallen, for their hospitality, knowledge and support. Paula for the attempts at performing experiments, and for all the times I could share thoughts with the 4D-Fatigue working group. Michael and Paul for their critique and advise. And finally all those who I do not mention by name; those who distracted my mind with coffee and spirits, or with sports and games, when I got stuck and required to rewind the knot of thoughts in my head.

Bart Scheeren
Delft, October 2017

Μή, εἴ τι αὐτῷ σοὶ δυσκαταπόνητον, τοῦτο ἀνθρώπῳ ἀδύνατον ὑπολαμβάνειν,
ἄλλ᾽ εἴ τι ἀνθρώπῳ δυνατὸν καὶ οἰκεῖον, τοῦτο καὶ σεαυτῷ ἐφικτὸν νόμιζε.
Not to assume it's impossible because you find it hard.
But to recognize that if it is humanly possible, you can do it too.

from *Meditations*
by Marcus Aurelius Antoninus Augustus
as translated by Gregory Hays

Abstract

Research into multi-axial fatigue requires knowledge on the through time and thickness development of the propagating crack front. In order to provide this knowledge methods must be developed to monitor crack initiation and growth during a fatigue test. The acoustic emission method has been recognised as a possible means to this end.

Fatigue is a failure mode that is characterised by the accumulation of damage during cyclic loading. Fatigue initiates on the microscale as dislocation movement, and subsequently develops into crack growth and eventual failure. In the assessment of fatigue damage it is critical to estimate the remaining lifetime. Prediction models have been developed for uni-axial loaded joints. However in the field of multi-axial fatigue these models are inadequate. To improve upon these models knowledge is required on the development of the fracture during cyclic multi-axial loading.

The acoustic emission method is a procedure for non-destructive testing that is based on detecting elastic stress waves originating from changes in the microstructure of an object. In the industry two common applications of acoustic emission exist. One of these aims to extract insights into the severity of damage from waveform features, the other aims to localise and correlate acoustic events. Novel applications focus mainly on the improvement of these two fields. A state of the art method is proposed which aims to localise acoustic sources in small scale volumes as a means of imaging the crack front.

Localisation of the sources is performed using a time difference of arrive scheme, which is also known as multilateration. The accuracy of this scheme is highly dependent on the accuracy of the input parameters. Therefore the times of arrival, receiver positions and speed of sound must be established meticulously.

Extensive processing is required to transform the recorded acoustic emission data into a representation of the crack propagation. For this purpose a post-processing system has been developed which automates time of arrival picking, event building and event localisation. The developed system is an extension to the AMSY-6 acoustic emission measurement system developed by Vallen Systeme.

In order to validate the accuracy of the extended measurement system an experiment has been designed. In a volumetric geometry sources are simulated in order to assess the bias and the variance, additionally noise is added to the simulation to evaluate the sensitivity of the procedures.

The study has shown that, under ideal noise conditions, the precision can amount to a cluster of about a millimetre in size. Additionally the bias of this cluster can be reduced to a minimum by means of careful calibration of the receiver positions and the speed of sound. Both of these observations indicate that an accurate representation of the propagating crack front may be obtained through a regression model, if the conditions are known and within acceptable limits. Regarding non-ideal conditions the analysis of the noise sensitivity has shown that the accuracy is relatively stable as long as the signal to noise ratio is kept above $SNR \geq 30$ dB.

In conclusion this has shown that monitoring the propagation of the crack front using volumetric acoustic emission source localisation may be possible if the conditions are right. This means that the signal to noise ratio must be kept above $SNR \geq 30$ dB. If this is the case, and if enough events are recorded to perform regression both the bias and the variance should pose a problem to monitoring crack growth.

List of Abbreviations

The following list contains the significance of all abbreviations used throughout this report. The page number refers to the page where the abbreviation is declared.

Abbreviation	Indicating	Page
AE	Acoustic Emission	1
AIC	Akaike Information Criterion	66
BK	Baer & Kradolfer	67
DT1Xm	First Hit Maximum Time Difference	33
DTnXm	Previous Hit Maximum Time Difference	33
ER	Energy Ratio	65
FHCDT	First Hit Channel Discrimination Time	33
HC	Hinkley Criterion	66
JIP	Joint Industry Project	1
LUCY	Location Uncertainty	15
MA	Maximum Amplitude	64
MER	Modified Energy Ratio	65
MSE	Mean Square Error	2
NDT	Non-Destructive Testing	1
PSB	Persistent Slip Band	9
RMSE	Root Mean Square Error	15
RPA	Receiveral Position Algorithm	31
SNR	Signal to Noise Ratio	31
SQL	Structured Query Language	34
STALTA	Short Term Average Long Term Average	64
TDOA	Time Difference of Arrival	13
TOA	Time of Arrival	13
TRAI	Transient Index	32
TU Delft	Delft University of Technology	1

List of Symbols

The following two lists contain the significance of all symbols used throughout this report.

Greek

Symbol	Usage
α	Hinkley Criterion Scaling Factor
Δ	Range Difference
ε_p	Error on Transducer Placement
θ	Unknown Parameter
$\hat{\theta}$	Estimator of Unknown Parameter θ
λ_1	Wavelength of Particle Wave
ν	Poisson Ratio
ρ	Density

Latin

Symbol	Usage
AIC	Akaike Information Criterion
BK	Bear & Kradolfer Criterion
c	Speed of Sound (Signal Velocity)
D	Dissociation Energy
DT1Xm	First Hit Maximum Time Difference
DTnXm	Previous Hit Maximum Time Difference
e	Envelope Function
ER	Energy Ratio
f	Frequency
f_{HP}	Hight-Pass Cut-Off Frequency
f_{LP}	Low-Pass Cut-Off Frequency
f_{op}	Operational Frequency (Range)
f_{res}	Resonant Frequency
f_S	Sampling Frequency
FHCDT	First Hit Channel Discrimination Time
G	Gain
h	Planck's Constant ($6.626 \cdot 10^{-34}$ Js)
HC	Hinkley Criterion
k	Allen Weighting Constant (k=3)
K	Bulk Modulus
LUCY	Location Uncertainty
MER	Modified Energy Ratio
r	Range
R^T	True Receiver Position
R^M	Measured Receiver Position
m	Atomic Mass
S^e	Estimated Source Space
S^E	Estimated Source Position
S^M	Measured Source Position
S^T	True Source Position
SNR	Signal to Noise Ratio

STALTA	Short Term Average Long Term Average
t_0	Time of Emission
t_a	Time of Arrival
$t_{\delta a}$	Time Difference of Arrival
T_{AD}	Duration of Pre-trigger Recording
T_{PD}	Duration of Post-trigger Recording
T_p	Peak Period
T_R	Duration of Recording
T_{SNR}	Signal to Noise Window
U	Output Voltage of Receiver
v_1	Broglie Relationship Velocity
v_f	Fitzpatrick Particle Velocity (Fracture Velocity)
V_1	Dilatational Plane Wave Velocity

List of Figures

List of Tables

Contents

1 Introduction

The chair of ship and offshore structures of Delft University of Technology (TU Delft) mainly focusses their research portfolio on the development of knowledge regarding fatigue and structural longevity. The 4D-Fatigue joint industry project (JIP) is one of their current research projects. It aims to develop fundamental knowledge regarding multi-axial fatigue in welded structural details. Within the 4D-Fatigue JIP another research project has been set up which addresses the interest for a crack front propagation monitoring method. This monitoring method is to be based on acoustic emission (AE); a non-destructive testing (NDT) procedure that utilises stress waves originating from microstructure rearrangement.

The goal of this thesis is to develop a volumetric acoustic emission fatigue crack monitoring system and to establish the limiting boundary conditions under which the system is capable of localising volumetric sources with millimetre accuracy.

This introduction addresses several topics regarding the structure and contents of this thesis. The upcoming three paragraphs discuss the approach by which the goal is brought within reach. Subsequently a major concept for this thesis, accuracy, is defined. Following up on this the difficulties regarding experimental research are elucidated. Finally the structure of the rest of this document is presented.

Road to Success. In order to reach the previously defined goal a set of questions must be defined which stepwise approach the end result. These questions are divided over two fields of study. The first is literature, which involves acquiring knowledge on the current state of the art, and, more explicitly, involves finding the knowledge gaps in the state of the art. The second is research, which involves the development of new knowledge to fill the gaps identified in the literature study. This process leads to an insight into the goal that has been set.

Literature. With respect to literature the main question is; what has been done before? In relation to the topics related to the research goal described in this thesis three questions have been identified.

The first of these is; which current generation inspection methods are used to monitor fatigue crack growth? It aims to discover which methods are usually applied to monitor fatigue crack propagation, and mainly to identify where the difficulties in relation to this lie with respect to the specifics of multi-axial fatigue.

The second question is; what are the current day applications of acoustic emission methods for structural health monitoring? This question aims to discover the capabilities of acoustic emission methods, specifically with regards to the mechanisms that relate to fatigue crack propagation.

The third and final literature question is; which knowledge gaps exist in the combined state of the art of these fields? It aims to discover where the research can expand on the current canon of acoustic emission fatigue monitoring.

Besides these three questions the literature study also serves the purpose to investigate the fundamentals regarding the involved topics. For this thesis the fundamentals of fatigue, acoustic emission methods and multilateration are considered.

Research. Based on the literature study and the exploratory study performed by Scheeren [23], a set of four research questions, aimed at bringing the goal within reach, have been identified.

The first of these is is; which methods can be utilised to improve automated processing of acoustic emission localisation? This question looks into the development of the acoustic emission post-processing system.

The second question is; what is the influence of a volumetric geometry on acoustic emission localisation? Through this question the effects of a three-dimensional geometry on the accuracy parameters are explored.

The third question is; what is the influence of noise on volumetric acoustic emission localisation? This question is aimed at uncovering the sensitivity of the implemented methods to noise.

The fourth and final question is; which boundary conditions must be met to accurately localise acoustic emission sources in a volumetric geometry? This question sets up the conclusion for this thesis, and aspires to leave a comprehensive guideline for application of the system.

Accuracy. The principal concept used in this thesis is that of accuracy. To assure a clear consensus on the definition of accuracy used in this thesis, it is explicitly stated. This definition follows ISO 5725 [10].

According to this norm accuracy is a combination of both trueness and precision. In this framework precision describes the closeness of individual measurement results to one another, whereas trueness describes the the closeness of the arithmetic mean of the measurement results to the reference value. As such precision accounts for a random error, and trueness accounts for a systematic error or a bias. To further elucidate the definition of accuracy figure 1.1 displays an illustration of the relation between trueness and precision.

In a statistical context the concepts of accuracy, precision and trueness are described by the mean square error (MSE), the variance and the bias respectively. An outline of mathematics involved with the relation between these concepts is presented in appendix A.

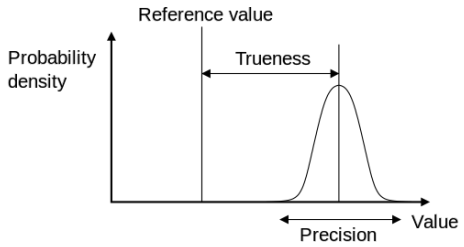

Figure 1.1: Accuracy components Trueness and Precision [35]

The Unpredictable Nature of Research. This thesis suffered from the unpredictability of experimental work. This required a change of scope in the later stages of the process. It would be inappropriate to dismiss this hardship, especially from a work of learning such as this, which is the reason why it deserves emphasis. Throughout this report several mentions are made to indicate changes relating to the change in the scope of work. This paragraph aims to fill in the blanks left by these mentions.

The original intent of the thesis was to adhere stronger to experimental results. As such the scope of work was specified to include the experimental activities of the 4D-fatigue JIP. However, due to the difficulties with the planning of this project, and the surprising results of the few experiments that had been performed, the scope has been redefined. Two main questions, that were part of the original intent of this thesis, are; which source localisation resolution can be achieved for data obtained from the specimen of the 4D-Fatigue JIP? And; how well does the acoustic emission method adhere to known fatigue crack propagation models?

These two questions adhere much more to the fatigue phenomenon, which was to be assessed through the experiments on the tubular and bar specimen. However, as was mentioned before, the few tests performed with these specimen did not yield the desired results. Overviews of the performed tubular and bar specimen experiments are included in appendices C and D. These appendices present the procedures, results and a discussion upon these results. Their contents were originally planned as the main matter for this report.

Structure. This report is structured around three modules, which provide a framework for the thirteen chapters and four appendices enclosed within these pages. To ease navigation through all of these the following paragraphs provide a basic guide. A more in depth description of the contents is included in the individual introductions of each of the chapters and modules.

Module I, Literature, covers a literature study, which includes chapters 2 to 6. It starts of with an introduction of the literature module in chapter 2. Followed in chapter 3 by the fundamentals required for this study. The state of the art is discussed in chapter 4, from which the knowledge gap is distilled in chapter 5. To complete the module it is concluded upon in chapter 6.

Module II, Research, covers the practical and experimental research. Enclosed in this modules are chapters 7 to 10. The first of these, chapter 7, provides a more specialised introduction to the research module. The second, chapter 8, elucidates on the acoustic emission measurement and post processing system. Experiments are covered in chapter 9, which describe the simulation methods and results used to define the boundary conditions required for accurate localisation. A conclusion regarding the research module is drawn in chapter 10.

Module III, Reflection, differs slightly from the others in a sense that it does not present any new information, but instead looks back to the study that has been performed and evaluates the effectiveness. Chapter 11 kicks the reflection off with a union of the conclusions drawn in the literature and research modules. Following on this chapter 12 discusses this conclusion in the framework of the intentions that have been laid out previously in this introduction. Based upon this discussion a set of recommendations are made for further research in chapter 13, which finalises the main matter of this thesis.

The unnumbered sections, the appendices, and the introduction of this first chapter are not contained within any of the three modules. The purpose of their presence is self-explanatory, and, with exemption of the appendices, needs no further elaboration. The appendices take a somewhat unique position. They are related to either the literature or research modules; describing additional topics deemed to be relevant to the study, though not to be of vital importance. As such the appendices will be more properly introduced in the modules for which they have been supplemented.

I

Literature

2

Introduction

The basis of research is research. A sentence which may seem either profound or superficial. The intend of this statement is to show that each research, most certainly in the current age, is preceded by the entirety of discoveries and observations forming the current state of the art. And the fact that research adds something to the knowledge of the current state of the art is exactly what defines research. Therefore it is crucial to build a scientific study upon a foundation of that what has been done before.

A literature study serves the purpose of assuring that research remains a field of knowledge development, rather than knowledge reproduction. In this report the literature study is composed of three parts.

The first part, contained in chapter 3, explores the fundamentals of the topics that come together in this thesis. The chapter elaborates on theories and concepts that have been part of the scientific canon for an extended period of time. For this these the fundamentals of fatigue, acoustic emission and multilateration are considered. The fundamentals of fatigue are covered to understand the mechanisms that lie at the basis of fatigue crack development, and to understand how acoustic emission can tie into these mechanisms. The fundamentals of acoustic emission are considered since acoustic emission is the main topic of this thesis, and thus deserves elaborate investigation. Finally the fundamentals of multilateration are considered because it is an essential technique for source localisation of recorded acoustic emission data.

The second part of the literature study considers the state of the art. This part is contained in chapter 4. Unlike the previous part this chapter only considers the cutting edge applications and discoveries in the considered fields of study. It aims to show the current limits to the available knowledge, and provide a starting point for further development. This chapter covers acoustic emission monitoring techniques aimed at structural health monitoring as well as an analysis of several novel waveform processing schemes.

The third part of the literature study, contained in chapter 5, identifies the knowledge gaps and elucidates the means by which this thesis aims to fill these. It provides a basis to justify the research questions that have been identified in chapter 1.

Finally a conclusion is drawn on the literature study in chapter 6.

3

Fundamentals

This chapter explores the fundamentals of fatigue, acoustic emission and multilateration. It discusses the main principles of these topics that are part of the established scientific canon.

3.1. Fatigue

Fatigue is a failure mode characterised by the accumulation of damage due to cyclic loading [24]. It is a failure mode that is present when a structure is continuously loaded by a varying stress that is below the yield strength of the considered material. The process of damage accumulation due to this stress variation can be subdivided in three stages. In order of occurance these are crack initiation, crack growth and failure. Figure 3.1 displays these stages and the mechanisms that contribute to them.

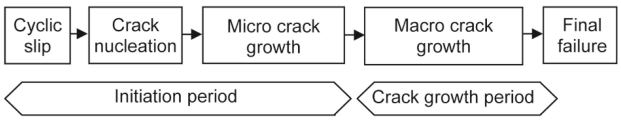

Figure 3.1: Stages of Fatigue Fracturing [24]

In the early stage of initiation cyclic slip leads to the development of persistent slip bands (PSB). It is a process governed by dislocation movement, and as such requires a shear stress. Dislocation movement occurs below the yield stress, or elastic limit, and is often referred to as microplasticity; derived from the fact that on microscale atomic rearrangement is considered to be a form of plasticity, though on macroscale it occurs in the elastic range of the material. The result of the formation of persistent slip bands is a surface roughness of exclusions and inclusions, as depicted in figure 3.2.

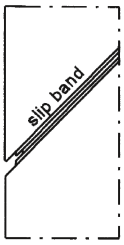

Figure 3.2: Persistent Slip Bands for Axial Tension [24]

This surface roughness introduces micro stress concentrations in the material, which nucleate cracks. This in turn leads to micro crack growth. Each of these mechanisms is dominated by the initial surface quality, the local grain geometry and imperfections present in the material. The dependency of the mechanism on the local geometry and properties is what sets the initiation phase apart from the crack growth period. The second stage of fatigue crack development is instead governed by the material bulk qualities. The crack growth

period is characterised by macro crack growth. It is typically much faster paced than the initiation period and of increasing intensity until final fracture.

An important factor in the assessment of fatigue damage is the measure of the remaining lifetime. Current generation fatigue crack growth and lifetime prediction models are predominantly developed for uni-axially loaded welded joints. These types of joints and loadings are representative for most fatigue sensitive locations in ship and offshore structures, though complex loading by wind and waves in combination with new exotic structural designs might introduce a multi-axial loading in a joint. For multi-axially loaded joints Sonsino and Kueppers have shown a significant reduction in the lifetime compared to uni-axially loaded joints [28]. Further research is necessary in order to establish the effects of multi-axiality on fatigue.

An inherent difficulty with research into multi-axial fatigue is the fact that multiple loading conditions are combined. As such it is very likely that at a certain time during an experiment a crack closing mode is combined with a shear mode. Such a situation would polish the growth bands that are commonly used to determine the crack growth rate [24]. Growth bands originate from the variation of the load level, and in dormant cracks from oxidation. They are elliptically shaped discolourations of the fracture plane, and as such often referred to as oyster-shell or beach markings. Without this means of a posteriori crack rate inspection, an alternative method to monitor the propagation of a fatigue crack is needed.

3.2. Acoustic Emission

The use of acoustic emissions, or microseismic activity, to assess the condition of an object dates back far into the history of man. One of the first professional applications of acoustic emission assessment might be that of potters, who used to listen to the clay pots cooling in the kiln with the intent of discovering unobservable cracks and weaknesses [6]. Baked pottery dates back 8,500 years.

With respect to metals tin cry is often regarded as the first observation of acoustic emission [6]. Tin cry is an audible sound produced by pure tin during twinning. The first observation of this type of acoustic emission is related to the first smelting of pure tin. It is often attributed to the craftsman who made the oldest known pure tin bangle, which has been dated to be from before 2,550 BC. Some 3,300 year later tin cry will also become the first documented observation of acoustic emission, when it appears in the work of the eight century alchemist Jabir ibn Hayyan.

In more recent history the term acoustic emission will eventually pop up. It is first used by B.H. Schofield in 1961 [7, 25], though J. Kaiser is often regarded as the father of modern acoustic emission research. Some ten years before Schofield coined the term acoustic emission, Kaiser published his dissertation on what he named acoustic phenomena [11]. For this study he performed experiments to investigate which noises metals generate when they are subjected to tensile stresses. The dissertation included a description of the Kaiser effect, which states that during repetitive loading dislocations will only move when, and thus elastic stress waves will only be emitted if, the previous load level has been exceeded.

In the world of today acoustic emission is typically utilised to monitor system integrity and production processes. The first of these is of specific interest in relation to this thesis. Typical applications in the field of integrity monitoring aim to detect sources, such as crack growth or dislocation movement, or pseudo-sources, such as leakage or friction. Each of these (pseudo-)source mechanisms generates acoustic emissions, which may be recorded by sensitive transducers. The fact that AE is about listening to the acoustics that are generated by inspected system itself, makes it a passive NDT procedure. Another unique feature of AE within the field of NDT is that the required plasticity to excite sources, is irreversible, and thus inherently destructive.

Phonon Fission. In metals stress waves are primarily generated by plastic processes and crack growth [21]. Both of these are characterised by rearrangement of the crystal lattice, requiring the breaking of atomic bonds. The energy related to the breaking of these bonds may be calculated through the theory of phonon fission. Phonons are quasiparticles that describe the quantised vibrational mode of interacting particles. In case an atom were to be removed from a lattice, breaking the atomic bonds would annihilate the phonon. This fission will be accompanied by a dissociation energy D equal to [5]:

$$D = mc^2 \tag{3.1}$$

A keen eye may notice that this equation for the dissociation energy is very similar to Einstein's famous equation describing the mass-energy equivalence. Though the difference is that in this equation c represents the

mean velocity of sound, instead of the speed of light. Additionally m refers to the atomic mass of the particle being removed from the lattice.

The dissociation energy presented in equation 3.1 provides an overestimation of the released energy during atomic rearrangement. Instead of removing the atom form the lattice, requiring all of the bonds to be broken, plasticity or fracture requires only that the bonds on the slip plane are broken. As such the released energy is only the fraction of the dissociation energy related to breaking that single bond. For this "partial phonon fission" the released energy is typically equal to $(^2/_3)D$ [21].

Another important factor to the generation of acoustic emissions is the fracture velocity, which determines the time-scale by which the energy is released. One assumes that the fracture velocity is equal to the Fitzgerald particle velocity for lattice disintegration given by:

$$v_f = \sqrt{v_1 c} \tag{3.2}$$

This equation states that the fracture velocity v_f is dependent on the mean speed of sound c and the de Broglie relationship velocity v_1. The last of these two can be derived from the relationship described by Louis de Broglie [4] as follows:

$$v_1 = \frac{h}{m\lambda_1} \tag{3.3}$$

In this equation h denotes Planck's constant ($6.626 \cdot 10^{-34}$ Js), m again represents the atomic mass, and λ_1 describes the wavelength of the particle wave. This wavelength λ_1 is equal to twice the distance of the closest approach of the atoms in the slip direction.

Solving these equations would show that the fracture velocity is much smaller than the stress wave velocity. This implies that the wavelengths of the stress waves will be proportionally greater than the size of the fracture event, the latter of which comes close to the grain size. This means acoustic emission wavelengths are a multitude of the grain size of a material. As such their propagation is not influenced by the crystalline structure.

Types of Waves. When fission deposits an amount of energy into an infinite solid elastic stress waves are generated. Two volumetric wave types are identifiable [6]. One of these is a dilatational wave, and as such similar to acoustic waves in gasses and fluids. Dilatational waves are characterised by particle movement along the direction of propagation. This type of wave is often referred to as a pressure wave and in some cases also as the primary wave, both are typically shortened to P wave. The other wave is a distortional or equivoluminal wave, and is often referred to as a shear, the secondary or an S wave. As such it is unique to solids due to their ability to transfer a shear force. The particle movement of a shear wave is perpendicular to the propagation direction. Both of the wave types are depicted in figure 3.3.

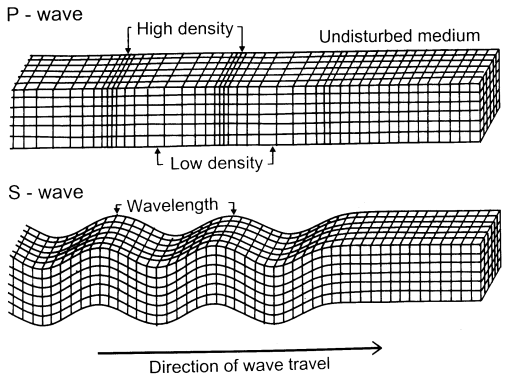

Figure 3.3: Pressure Wave (P) | Shear Wave (S) [12]

If P and S waves were to interact with the surface of a one side bounded solid, another type of wave will develop. This developed surface wave is a Rayleigh wave, which contains both a longitudinal and a transverse component. As such they are characterised by cyclic particle movement, which is also depicted in figure 3.4.

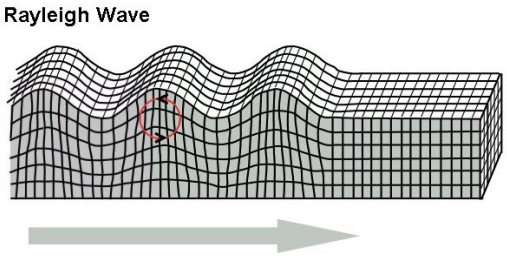

Figure 3.4: Rayleigh Wave [34]

A special type of Rayleigh wave exists for a solid bounded by two closely spaced parallel surfaces. In this case a plate wave will develop, which is referred to as a Lamb wave. Lamb waves exist in a wide variety of modes. The dominant two of these are the zero-order symmetric S_0 and antisymmetric A_0 modes, most higher order modes carry only very little energy and are thus often unobservable. Figure 3.5 illustrates on the symmetry or antisymmetry of Lamb waves.

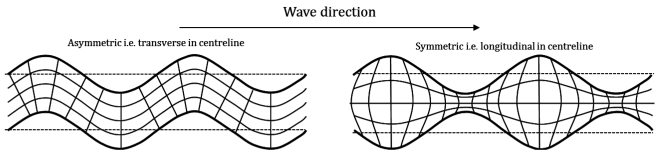

Figure 3.5: Lamb Wave Modes | Antisymmetric (left) | Symmetric (right) [16]

Volumetric and Rayleigh waves are expected to be encountered in the experimental work performed for this thesis, since only bulky specimen are considered. With respect to the experiments performed for the 4D-Fatigue project, Lamb waves may be expected to develop along the circumference of the tubular specimen.

Feature Extraction. In the early days of acoustic emission research the data storage capacity was limited. This meant only certain waveform parameters, known as features, could be stored, instead of the actual wave form. These features aimed to best capture the shape and content of the waveform. Recent improvements in information technology have allowed for the storage of large numbers of transient signals associated with acoustic emission research. This provides the option to perform a more in depth analysis of the signal, which has lead to an increase in the effectiveness of acoustic emission methods.

A typical acoustic emission waveform with some of the classical features is presented in figure 3.6. This figure is used to elucidate on a variety of features commonly used for waveform characterisation, some of which are also depicted in the figure.

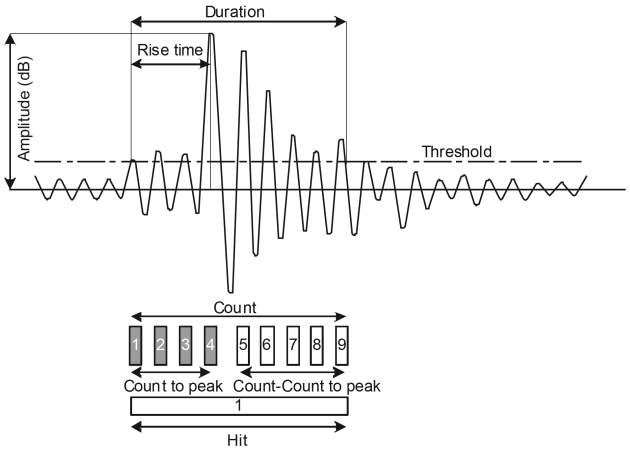

Figure 3.6: A Typical Acoustic Wave and Several Features [7]

The following features are commonly evaluated in acoustic emission research:

Time of Arrival. The time of arrival defines the onset of the acoustic wave. It is determined as the first sample of a signal crossing a certain threshold. It is defined to be the start of a hit.

Peak Amplitude. The peak amplitude of a hit is the largest absolute signal value for a recorded waveform. It is recorded in the order of µV and typically represented in a decibel scale (dB_{AE}). The reference value for the calculation of this decibel scale is $U_0 = 1$ µV.

Rise Time. The rise time of the hit is the time interval between the first threshold crossing and the peak amplitude.

Duration. The duration of a hit is defined to be the time interval between the start and end of a hit. The end of a hit is typically determined as the threshold crossing preceding a set duration discrimination time without further threshold crossings.

Counts. Counts are defined to be the number positive threshold crossings occurring for the duration of the hit. The limitation to only positive threshold crossings might lead to situations where a hit contains 0 counts, this would be the case for a hit composing of a solely single negative threshold crossing.

Energy. The energy of the hit is defined to be the integral of the squared signal. It is determined discretely by summing the squared sample values for the duration of the hit and multiplying this value with the sampling time.

Signal Strength. The signal strength of the hit is defined to be the integral of the signal. It is determined discretely by summing the sample values for the duration of the hit and multiplying this value with the sampling time.

RMS Noise. The root mean square noise is a measure of the background noise. It is typically calculated from a short sample of signal values in the period between two hits.

Cascaded Hits. Cascaded hits are multiple hits arriving in close succession. They are typically regarded to originate from a single source event. Cascaded hits arrive after the duration discrimination time has passed, and thus do not belong to the recorded hit, but do arrive within the rearm time, which is set to distinct hit sets. For cascaded hits features like the counts, energy and signal strength are often calculated.

3.3. Multilateration

Multilateration is a source localisation scheme based on the time differences of arrival (TDOA) of a signal at different receiving stations. In order to understand the solution to the multilateration problem it is of essence to know what constitutes, and is implied by, the recorded time difference of arrival. To elucidate this a receiver in a three-dimensional space is defined:

$$R^T = (x_R, y_R, z_R) \in \mathbb{R}^3 \tag{3.4}$$

At a certain time this receiver observes the arrival of a signal. This time of arrival (TOA) is governed by:

$$t_a = t_0 + \frac{r}{c} \tag{3.5}$$

Which shows that the time of arrival t_a is dependent on the unknown time of emission t_0 and the travel time; the last of which is denoted in this equation by the fraction of the range r and the known signal velocity c.

The range describes the distance the signal has travelled, thus the distance between source and receiver, which is determined as given:

$$r = \|S - R\| \tag{3.6}$$

In this equation $\|\ldots\|$ denotes the Euclidean norm.

S describes the source position, which is expressed as:

$$S^T = (x_S, y_S, z_S) \in \mathbb{R}^3 \tag{3.7}$$

The three Cartesian coordinates of this source, and the time at which it emits the signal are the four unknowns in the time of arrival problem of the considered receiver. This receiver provides a single equation, and as such

it becomes clear at least four arrivals at uniquely situated receivers are required to locate a source position in three dimensions, and, if wished so, to determine the time of emission of the signal.

However, the exact time of emission is often not of interest. As such multiple arrivals of a single event at different receivers can be used to eliminate the unknown arrival time from the equation. To this purpose the time differences of arrival are calculated. In an isotropic medium this leads to the following:

$$t_{\delta a_{i\to j}} = t_{a_j} - t_{a_i} = \frac{r_j - r_i}{c} \tag{3.8}$$

The time differences of arrival represents the difference in the travel time of the signal between two receivers. Typically the first arrival of a signal, or first hit, is used as the basis for the TDOA calculation ($i = 1$).

Since multilateration is a localisation problem the solution is sought in the spatial domain, rather than the time domain. The transfer to the spatial domain is performed through multiplication of the TDOAs with the signal velocity; the resulting equation is:

$$\Delta_{i\to j} = c\, t_{\delta a_{i\to j}} = r_j - r_i \tag{3.9}$$

The difference it describes is referred to as the range difference.

Using this range differences a hyperboloid sheet can be constructed between the associated two receiver stations. This hyperboloid sheet includes all possible source locations for the signal recorded at both receivers. Effectively the addition of a second receiver to the receiver grid reduced the possibility of the location of S from the whole of $\mathbb{R}^3$ to a plane in that space. Adding another receiver to the receiver grid will provide another TDOA set, and thus also a set of hyperboloid sheets. These three sheets intersect on a single line, which will somewhere include S. Even though a new receiver adds multiple new TDOAs and hyperboloid sheets, only a single new unique solution is obtained. The reason for this is that TDOAs are only combinations of a basis which is made up by the receiver coordinates and the arrival times. No new data is added by making different combinations, the data is just represented differently. To find the source on the aforementioned line a fourth receiver needs to be added to the grid, which yields more TDOAs, allowing for the construction of three more hyperboloid sheets. All of the six sheets intersect in a single point defined as S.

A case of two-dimensional localisation using four receivers is shown in figure 3.7, as a means of illustrating the localisation problem. This figure shows four receivers and the six hyperboloid sheets that can be constructed from the TDOA combinations of these four receivers.

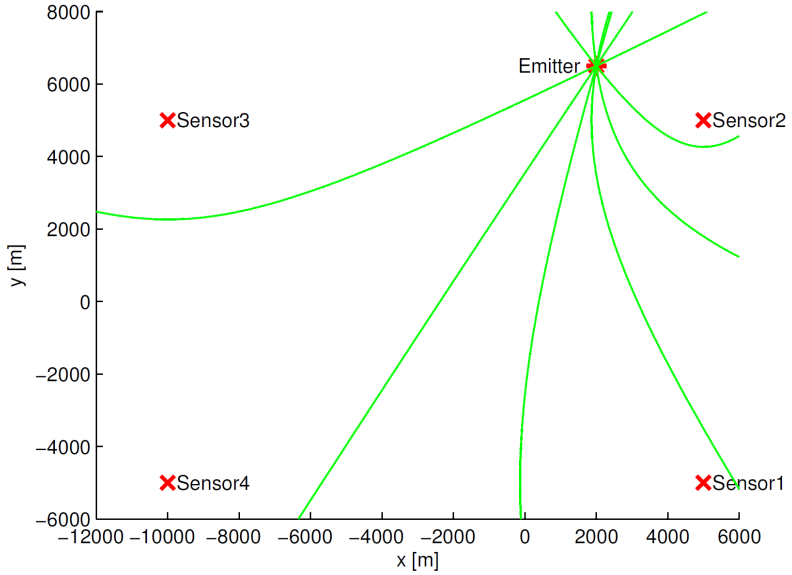

Figure 3.7: Intersecting hyperboloid sheets of TDOA-based source localisation [29]

The described case where six hyperboloid sheets intersect in a single point is one that omits any disturbance in the input parameters. The difficulty with multilateration is that a measurement error in the time of arrival, the receiver positions or the signal velocity often leads to non-intersecting hyperboloid sheets. As such obtaining the source location becomes a minimisation problem, the goal of which is to find the most likely source location.

A means to finding the most likely source location is the location uncertainty (LUCY). This measure is used in the acoustic emission event localisation algorithms developed by Vallen Systeme [30]. The LUCY is defined as:

$$\mathrm{LUCY} = \sqrt{\frac{1}{J-1}\sum_{j=2}^{J}\left(\Delta^{e}_{1\to j} - \Delta^{m}_{1\to j}\right)^{2}} \tag{3.10}$$

This equation shows that the calculation of the LUCY is similar to the calculation of a root mean square error (RMSE). It describes the calculation of the LUCY as the error between the the measured range differences Δ^m and the estimated range differences Δ^e, which are determined using an estimated source space S^e. For each of the range differences the first arrival is used as the base of the calculation, all subsequent arrivals are cycled through ($j \in [2 \dots J]$).

The LUCY describes the measure of unfit of the solution space with respect to the measured data. The most likely source position corresponds to the point where the LUCY is minimised, as described in:

$$S^E = \underset{S^e}{\arg\min}\left[\mathrm{LUCY}\left(S^e\right)\right] \tag{3.11}$$

This equation states that the best estimated source position S^E is equal to the argument of the minimum of the LUCY. A decent multi-variable non-linear minimisation algorithm is necessary to solve this equation. Since these algorithms are available in the canon of mathematics the localisation problem is considered to be solved.

4

State of the Art

This chapter presents the state of the art in acoustic emission technology. On one side it discusses novel methods of structural health monitoring, on another it looks at new signal processing methods.

4.1. Acoustic Emission Techniques for Structural Health Monitoring

A common application of acoustic emission within the field of structural health monitoring is to detect crack development. In general the research in this field can be subdivided in two camps based on the approach of the problem. On one side there is feature research, on the other side there is localisation research.

Feature research aims to assess the severity of the damage by means of analysis of the waveform parameters. An example of a recent success in this field is a study which found distinctions in the AE signals of concrete anchor pull-out tests. These distinctions may allow for prediction of the fracture mode [18]. In this case identification of the fracture mode can be used to classify the defect as critical or non-critical to the reliability of the structure.

A slightly older study evaluated the acoustic signals recorded from a mooring chain undergoing cyclic loading [13]. They identified differences between crack initiation, crack propagation and final fracture in several waveform features. These differences allow for a better prediction of the remaining lifetime, and may thus lead to optimised maintenance.

The field of localisation research is mainly aimed at a larger scale. The goal is to identify the location of damage on a structure, rather than to assess the severity of this damage. Recent improvements in this field relate to mitigating the adverse effects of complex thin walled geometries on wave propagation to further improve localisation in assembled structures [20]. Decent location results in this field of study are typically in the order of decimetres.

In contrast to these two common applications of acoustic emission there are also some attempts to explore new possibilities. These studies are aimed at localisation on a smaller scale. Ronde et alii performed a study in which they attempted to localise sources coming form a microfracture event in an olivine sample with a length of 3 mm and a diameter of 1.6 mm [22]. More than 95% of the localised sources were placed within an ellipsoid with a length of 3.6 mm and a diameter of 1.6 mm.

4.2. Novel Time Picking Methods

Proper selection of the time of arrival is most critical to the localisation of an acoustic emission event. Therefore extensive research has been performed into automated onset detection methods. Appendix B covers a wide range of established time picking methods, which are all limited to the time domain.

In more recent years, with the increase of computational resources, frequency domain time pickers are becoming of interest. The wavelet transform, which contains both frequency and time information, is particularly suitable for this process. Recently a comparative study into several time-frequency and time domain pickers has been performed by Bai et alii [3].

For their study they developed two continuous wavelet transform based time picking functions, which they compared to two time domain time pickers and threshold picked arrival times. The comparison was made based on data from a fatigue crack growth test performed on a specimen subjected to uni-axial tension. A single edge notch served as the initial defect.

In general the time-frequency domain time pickers performed better on both the precision and accuracy, in this study represented by the mean absolute error, than the time domain time pickers. However this improved result came at the cost of a significantly increased computational effort.

Because of the required computational effort per hit continuous wavelet based time pickers are currently unsuitable to process large samples of events, especially for extensive receiver configurations. Therefore they have not been implemented in the post-processing system developed in this thesis.

5

Knowledge Gap

This chapter aims to identify which knowledge gaps are present in the state of the art. It is aimed more specifically at acoustic emission methods for fatigue monitoring, and at problems with the trueness that have been identified in exploratory work.

5.1. Acoustic Emission Methods for Fatigue Monitoring

In order to investigate crack propagation in experiments involving multi-axial fatigue a method is required to monitor the development of the crack front in real time. The acoustic emission method is theoretically suitable for this task, since it deals with the elastic stress waves generated by plastic events and lattice disintegration, both of these phenomena are associated with the propagation of a crack front.

This hypothesis is yet to be proven, since common acoustic emission methods are involved with either large scale localisation, or small scale feature analysis. However, a study by Ronde et alii shows that small scale volumetric localisation has potential for accurate results [22].

An exploratory study by the author has already shown that a high precision is obtainable for planar localisation [23]. These results are to be validated for a volumetric situation and to be expanded for noise sensitivity.

5.2. Correction of Trueness

An issue that was identified in the exploratory study was that the bias of acoustic localisation is difficult to assess [23]. In order to correctly assess the bias a high accuracy on the placement of both receivers and sources is required. A clear approach to investigating the bias of acoustic localisation should be developed. Subsequently a method to correct for this bias should be proposed.

6

Conclusion

This literature study aspired to discover what had been done before in the fields related to the research question. The greater goal of this aspiration was to identify where this research might fill the gaps in the current knowledge. In the previous chapters it has done so by elaborating on the fundamentals, by exploring the state of the art and by identifying the knowledge gap.

Regarding the fundamentals fatigue is discussed for both the fracture mechanics and propagation monitoring methods. These tie into the basics of acoustic emission, which starts off with an overview of the history of acoustic emission observations and applications. The knowledge on acoustic emission is expanded to the physics behind the generation of stress waves through a peripheral evaluation of phonon fission and lattice disintegration. Subsequently the different types of waves are mentioned, and broken down into several characteristic features. The assessment of the fundamentals finally covers the basics of the maths behind multilateration, in order to show the parameters which influence the accuracy.

Starting from this foundation the literature study explores the state of the art. On one side it looks at the current applications of acoustic emission in structural health monitoring, which shows that small scale volumetric source localisation is a cutting edge application that deserves in-depth research. The other side of the state of the art evaluation looks for novel onset detection methods. In this field time-frequency domain functions based on the wavelet transform are the promising next generation of time pickers. However, these functions still lack the capacity to process a large number of waves as the computational requirements are intensive.

This study, and the exploratory study performed earlier, lead to the identification of some knowledge gaps. The first of these gaps focusses on the possibility to inspect fatigue crack propagation using acoustic source localisation. The second focusses on the accuracy of this source localisation, with a specific interest for the bias or trueness.

II

Research

7

Introduction

It is often said that one learns best from making mistakes. In case failure is considered to be a mistake this idea suits fatigue research exceptionally well. However, it also is a set-up for a paradox when one assesses the implication of failing to cause structural failure. Whichever may be best for learning is uncertain. What is certain is that the latter of the two resulted in the study presented in this module.

This chapter serves the purpose of presenting the knowledge that has been developed over the course of the project. As a result of the change in the scope this research is subdivided into two parts. Two appendices cover a part of the research related to the original scope.

The first part of the research contains a description of the acoustic emission measurement system and the development of the post-processing system. This part can be found in chapter 8. The chapter starts off with an in depth description of the AMSY-6 acoustic emission measurement system, which has been used as the basis for the volumetric fatigue crack monitoring system. It covers the basics in the terminology and principles of acoustic emission measurement equipment, and specifies which specific hardware has been used for this project. Following on this the shortcomings of the off-the-shelf system are identified, and the requirements of the post-processing system are outlined. Based on these requirements the post processing system has been implemented, which is described in the next section, this also covers an insight into the operability of the system. A final section in the chapter describes the database created to store processed data, and shortly mentions the formats and interfacing.

The second part, contained in chapter 9, describes the validation of the acoustic emission measurement system by means of a simulation study into the accuracy and boundary conditions. It discusses the methods used, focussing on the design of the specimen and the simulation approaches. Subsequently calibration is performed to improve the quality of the result and observe initial signs of inaccuracy. The following section presents and discusses the result from the simulations. Based on these the chapter closes with a set of boundary conditions to localisation.

To finalise the research conclusions are drawn in chapter 10.

Besides the research presented in these chapters several attempts have been made to apply the volumetric acoustic emission fatigue crack monitoring system to monitor crack development in the tubular and bar specimen of the 4D-Fatigue JIP. However, all but one of these tests have been unsuccessful in a sense that no visible fatigue crack developed in the specimen. This eventually lead to the conclusion that a change in the scope of the project was necessary in order to validate the measurement system, the result of which is presented in chapter 9. The methods are results related to the experiments with the bar and tubular specimen are included in appendices C and D respectively.

8

Acoustic Emission Measurement & Post-Processing System

The most crucial aspect of acoustic emission research is recording acoustic emission signals. The second most crucial aspect to acoustic emission research is post-processing of the recorded acoustic emission signals. The ability to achieve both of these is discussed in this chapter. Both the off-the shelf acoustic emission measurement system and the extended post-processing system are discussed. The intent is to develop an understanding of the hardware and software associated with the tests that are performed in upcoming chapters of this thesis.

To record acoustic emission signals the AMSY-6 acoustic emission measurement system developed by Vallen Systeme will be used. It is described thoroughly in section 8.1.

In order for the intended results to be delivered this of-the-shelf acoustic emission measurement system must be expanded upon. To this purpose a post-processing system will be implemented. An outline of the requirements and structure for this post-processing system are defined in section 8.2. It is followed by section 8.3, which describes the implementation of the post-processing system.

A database, which has been dubbed the secondary database, forms the core of the data infrastructure of the post-processing system. A clear description of the structure and contents of the secondary database is given in section 8.4.

8.1. Acoustic Emission Measurement System

The joint venture of Vallen Systeme and TU Delft has provided the project with a AMSY-6 acoustic emission measurement system. This system encompasses the whole of the hardware and software used in acoustic emission data collection and analysis. Figure 8.1 displays a diagram of the AMSY-6 acoustic emission measurement system. An important remark with this figure is that in this document, unlike in the figure, sensors are referred to as receivers. This wording has been chosen to better differentiate, both linguistically and mathematically, between sources and receivers.

The system in figure 8.1 displays only the components of the acoustic emission measurement system which have been provided by Vallen Systeme. The crux of this thesis is the development of an extension to the conventional system to further post-process the acoustic emission signals for the purpose of high accuracy source localisation. The extended acoustic emission measurement & post-processing system includes a second computer which interfaces with the one already present in the conventional system. This extra computer and the post-processing software running on it are what differentiates the extended acoustic emission measurement & post-processing system from the conventional solution that is currently on the market. The sections in this chapter which follow up on the current one further elucidate all of the subjects related to the post-processing extension of the AMSY-6 acoustic emission measurement system.

This section is intended to clearly illustrate the working principles of the AMSY-6 acoustic emission measurement system, and to indicate which hardware options have been selected for the research described in this document. To start with the first of these a case from source to recording is considered.

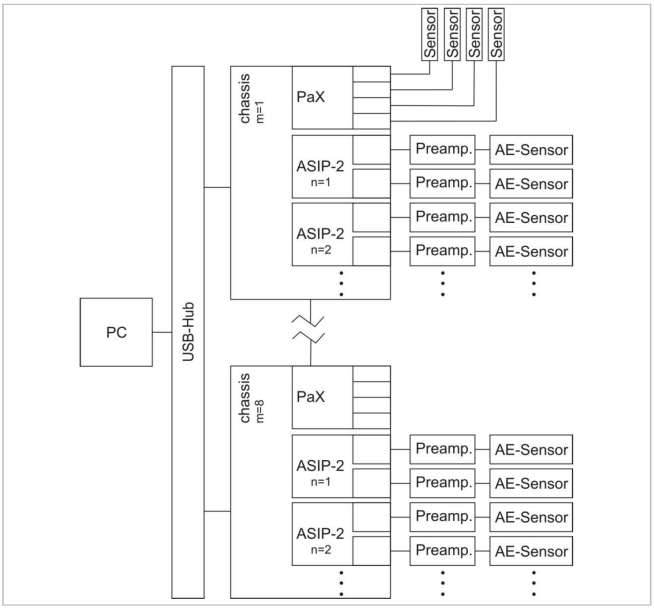

Figure 8.1: Overview of AMSY-6 acoustic emission measurement system [31]

An incident, either at the surface or inside of the material, deposits a certain amount of energy into the material. This energy is partially transformed into elastic stress waves; acoustic emissions. A receiver attached to the outside of the material encounters the minute surface deflection resulting from such an elastic stress wave. This deflection deforms the piezoelectric crystal inside of the receiver, which due to this deformation generates an electric signal.

This electric signal is fed into a pre-amplifier. This pre-amplifier can be either integrated with the receiver or situated externally. The purpose of the pre-amplifier is to provide initial filtering, to amplify the signal and to provide cable driving capacity.

The amplified signal is passed on to a signal processing card installed in the chassis. This card performs roughly four processing operations. As a first it passes the signal through an analogue band-pass filter to limit the considered frequency range to the frequency range of acoustic emissions. This additionally provides a means of anti-aliasing. Figure 8.2 illustrates the ASIP-2 analogue filter passband in relation to several types of acoustic signals.

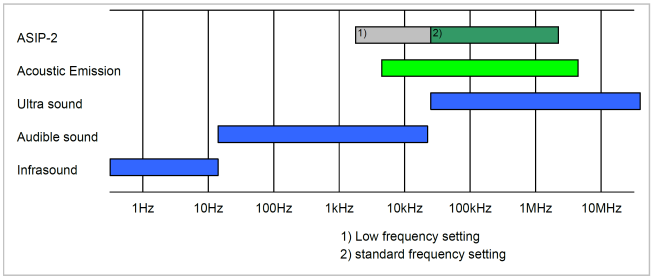

Figure 8.2: Overview of Recordable Frequency Ranges [31]

In the second stage the signal processing card performs analogue to digital conversion on the band-pass filtered signal. Inherent to this conversion is the noise it imposes on the signal. As such the third stage is focussed on reducing the noise by means of one of a wide variety of digital filters. This third stage can also be bypassed.

The final stage is related to the recording of the signal. It is the stage in which features are extracted from the waveform that is the result of the whole previous process. Which features to extract is a choice of the operator, though it will always include set-id, set-type, time of arrival and channel. Further options may also include threshold, amplitude, rise-time, duration, energy, signal strength, root-mean-square-noise, counts, and several cascaded parameters. A clear description of each of these features is given in section 3.2.

All features are stored in the primary database. The waveform itself may also be recorded in the transient database if the installed signal processing card contains a transient recorder. Both databases are based on a binary format and compatible with SQLite3.

Synchronous to acoustic emission signal processing the system also processes a number of optional parametric channels. In figure 8.1 these channels are indicated as PaX. Parametric data is stored together with feature data to provide a frame of reference to the acoustic emission activity.

The route from source to database is considered acquisition. It is governed mainly by hardware, and intrinsically by firmware. Control over the acquisition hardware and firmware can be exerted through the selection of specific hardware components, through mechanical switches accessible both externally and internally, and through the acquisition application of Vallen AE Suite Software. The latter of these provides an interface to control four functionalities related to data acquisition. The first of these functionalities is hardware detection, which is used by the system to verify the connected hardware. In this stage the user designates channel numbers and the attached pre-amplifiers. The second functionality is database specification, allowing for creating and writing database files. The third, and most critical to the format of the recorded data, is acquisition parameter specification. It can be used to specify, among others, the sample rate, the threshold, the use and settings of the transient recorder, the applied digital filters and the extracted feature data. The final functionality of the acquisition application controls data recording. It is used to start, stop or pause data recording, and may also be used to monitor and alter the threshold.

Acquisition only describes half of the potential of the AMSY-6 acoustic emission measurement system. The other half is provided by evaluation tools, which process available data to present the desired results. The core of this data processing is the VisualAE analysis program. This program acts as the primary data interface for both on-, and off-line operation[1]. The strength of this system lies in the customisability of processing tools and visuals, and in the direct feedback it provides.

However the existing system does have some limitations regarding the processes related to event localisation. This is where the extended acoustic emission measurement & post-processing system comes into play. The following sections of this chapter elaborate upon this.

Above the working principle of the AMSY-6 acoustic emission measurement system has been described. This working principle is subjected to certain system specifications. The following specifications are constants throughout all of the performed measurements.

Chassis. The considered chassis is an MB19. This chassis is suitable for standalone operation and is able to accommodate nineteen signal processing cards. For this project nine ASIP-2A signal processing cards have been installed, allowing for acoustic emission data acquisition with up to eighteen channels. Each of the channels contains a transient recorder which is able to sample at a rate of up to $f_S = 40\ MHz$. The analogue filters on each of the cards are set for standard frequency operation. As shown by figure 8.2 this indicates a passband ranging from a high-pass cut-off frequency of f_{HP} = 18 kHz to a low-pass cut-off frequency of f_{LP} = 2.4 MHz.

Receivers. For the project VS600-Z2 receivers have been selected [33]. One of the main factors in receiver selection was their size. Due to their diameter of d = 4.75 mm the VS600-Z2 receivers are realisable on small scale specimen. The size also imposes the absence of an integrated pre-amplifier. Additionally to their size these receivers have also been selected for their wide band sensitivity. The operational frequency rages from $400 \leq f_{op} \leq 800$ kHz, with the resonant frequency at f_{res} = 600 kHz. The piezoelectric transducer is encased in a full metal housing, which provides the ideal surface for a glue based interface with the specimen.

Pre-Amplifiers Since the receivers have no integrated pre-amplifiers this task is covered by external AEP5H acoustic emission pre-amplifiers [32]. These amplifiers have been set to a gain of G = 40 dB. An internal switch allows for changing this gain to a lower gain of G = 34 dB.

Acquisition. Like most of the hardware settings some of the acquisition parameters can too be considered constants. The most important of these is that all experiments will be recorded at a sampling frequency of f_S = 40 MHz for both feature and transient data. This sampling rate is chosen to provide a high resolution

[1] On-line; during acquisition | Off-line; after acquisition

in TOA selection, and thus in localisation. A limitation of this sampling rate is that only few digital filters are applicable to it, and that it amounts to sizeable transient recordings. A broad band-pass filter has been selected to filter only those frequencies that are outside of the receiver sensitivity. This filter is characterised by a high-pass cut-off frequency at $f_{HP} = 100$ kHz and a low-pass cut-off frequency at $f_{LP} = 1000$ kHz.

Some acquisition parameters need not be defined as constants, but do need to conform to a certain standard. This is the case for the amount of pre- and post-trigger samples, which dictate the duration of the recording before the first threshold crossing and after the last threshold crossing. To assure the possibility for all time picking functions to operate as intended, durations of at least $t_{AD} = t_{PD} = 200$ µs are required for the respective pre- and post-trigger recordings. At a sampling rate of $f_S = 40$ MHz both of these account for 8,000 samples. This also imposes a requirement on the sample page length, which would be that the minimal duration of a recording should be at least equal to the sum of the pre- and post-trigger durations.

8.2. Post-Processing Requirements

The AMSY-6 acoustic emission measurement system as is, is unable to perform up to the accuracy the research project requires of it due to threshold-based time of arrival selection. Therefore the system will be expanded with a post-processing system. In the current and the next two sections the whole of the post-processing system and the secondary database are elucidated. This section discusses the requirements and the structure of the post-processing system.

The intent with the post-processing system is to provide the ability of high accuracy event localisation. The starting point for this post-processing will be the acoustic emission data as it is recorded in the primary and transient databases. All further operations, which will eventually lead to a crack propagation representation, will be included with the post-processing system.

This intent describes the functional requirements of the post-processing system. In conjunction to these system specifications should be defined. A first of these requirements will be intrinsically satisfied. The acoustic emission post-processing system should be able to run independently of the measurement system. This is achieved by the separation of measuring and post-processing to dedicated computers, as was described in the previous section when the position of the post-processing system in the acoustic emission measurement system was made clear.

Another system specification is the requirement to operate on a start-stop-restart basis. Due to the possibility of a large amount of events the system should be able to process these events discontinuously. This requires the system to keep track of the post-processing status of all hits and events.

Similarly to this is the requirement that it should be possible to initiate each of the post-processing stages individually. This will allow for more effective post-processing, since each of the stages can be analysed before the next is initiated. Separating system modules to perform post-processing operations could achieve this system specification.

On the topic of functional requirements there are several stages to go through to obtain a crack propagation representation from the as-recorded primary and transient database files. Roughly this process can be divided in three steps, with localisation at the centre of them. The step before localisation covers input parameter acquisition, optimisation and preparation. The step after localisation covers constructing the crack propagation representation.

The main pillar in the data infrastructure of the post-processing system is long term storage of results in the secondary database. The format and structure of this database are extensively illustrated in section 8.4. However in this current section, on the requirements and structure of the post-processing system, and in the following section, on the implementation of the post-processing modules, references are only made to a superficial concept of this database.

As stated before the process of obtaining the crack representation can be divided in three parts, with localisation at the centre of these. Localisation in itself requires an algorithm to solve the LUCY problem that has been described in section 3.3. The choice of this algorithm has a great influence on the computational efficiency and the accuracy of the localisation process. Additional features of localisation are a front-end and a back-end filter. The front-end filter serves as a validation to check whether the event is of good quality. The back-end filter serves as a check to identify a possible bad localisation result.

The most important aspect of localisation is the quality of the input data. As such the part of post-processing preceding localisation, concerning with the acquisition and optimisation of input parameters,

is key. As was described when multilateration was elaborated upon, input consists of times, or time differences, of arrival, receiver positions and a speed of sound. Some of these parameters need to be specified by the user, others are derived from the recorded AE data.

The times of arrival will be determined by the post processing system from the waveforms contained in the transient database. For onset detection automated time picking functions need to be implemented. The system needs to be able to process multiple types of time picking functions for a single dataset. Methods of denoising are left out of the time picking effort; primarily because the noise typically parallels the AE signal in frequency content, secondarily because denoising is computationally intensive. Instead the signal to noise ratio (SNR) will be calculated to serve as an indication of the quality of the time pick. The quality of the time pick is to be stored in a logical value for the sake of filtering out bad time picks.

To acquire the time differences of arrival it is necessary to know which hits are correlated in events. This requires event building. Event building will be based upon the times of arrival as-recorded in the primary database. These TOAs have been chosen instead of the time picked TOAs since the slight difference in time picking should not alter event building. Instead event building can only be fine-tuned through a series of user defined parameters.

With respect to inputting speed of sound and receiver positions the requirements are consistently applied. Receivers coordinates need to be provided directly, or through a structured table processable by the receiver positioning algorithm (RPA) developed by Scheeren in his exploratory work [23]. An important addition to the table of receiver coordinates is a field specifying the usage of the receiver as either active, inactive or guard. Guard receivers will be used to isolate undesired acoustic emissions by means of blocking-off the system when they are triggered. The speed of sound is required to be individually specifiable for each set of time-picked data.

The final step of the data analysis is required to transfer the localised source data, by means of a regression model, into a format comparable to known fatigue crack propagation models. This step leads to a crack propagation representation. Since a feeling for the localised source data is necessary to consider the means of representing these data, the lack of these data halted further specification and development of the requirements, and later on implementation, of this part of the post-processing system.

8.3. Post-Processing Implementation

The post-processing system has been implemented in MATLAB. The five blue ellipses of figure 8.3 represent the five main modules which govern all mathematical operations. The white box, containing the crack propagation representation modules, has not yet been implemented, as was described in the previous section.

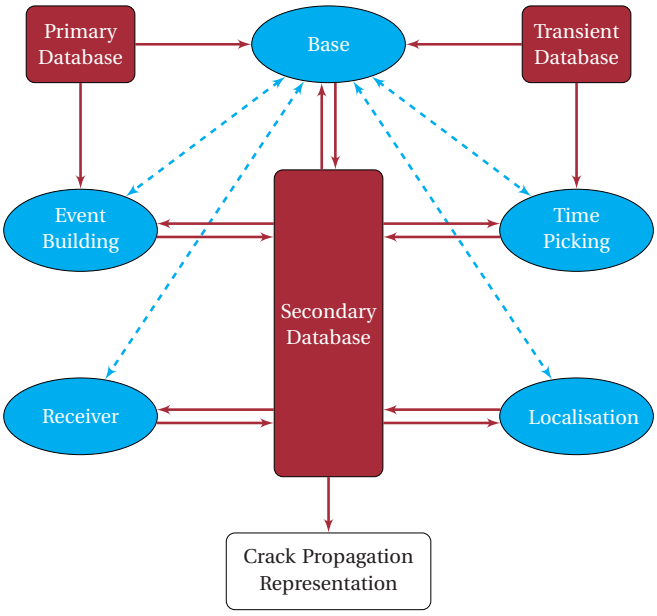

Figure 8.3: Overview of Post-Processing System

Base. The core of the post processing system is formed by the base module, programmed in the file *MasterBase.m*. It is programmed for database selection and verification, and to operate as a switchboard between other post-processing modules. Additionally feedback functions have been added which present the current status of time picking, event building and localisation.

A main functionality of the base module is the verification of matching contents of the secondary and primary and transient databases. It does so by comparing the transient indices (TRAI)[2] present in all of the databases, while taking the specification of a structured TRAI list into account. Irregularities in the comparison of these indices lead to one of two cases. Either new data is added to the secondary database if the primary and transient database contain more entries than those present in the secondary database, or the secondary database is marked as corrupt if it contains entries not present in the primary or transient database. The latter option requires re-creation of the secondary database.

Time Picking. The first of the modules that are selectable in the switchboard contained in the base module is the time picking module. This module is governed from the function *fMasterTimePicking.m*. The code of this file is subdivided in three parts.

The first part is dedicated to the selection of the time picking scheme, checking the database for existing schemes and inserting new schemes into the database.

The second part is designed to select and obtain the starting point for the time picking process and to select the desired runtime. The user can specify to either continue or restart the process. Selecting to continue time picking will instruct the system to find the index of the first unpicked hit, and to continue from thereon. Selecting to restart will instruct the system to delete the current time picking progress from the database, and to initiate time picking again at the first hit in the database. Subsequently to specifying the starting point the desired runtime needs to be specified. Reaching this time, or the end of the database, will instruct the system to halt and store the processed data.

The third part part of the code deals with time picking itself. Unless the option *No_No* is specified, to omit time picking and use the threshold based TOAs, this process will start with obtaining the waveform of the current TRAI from the transient database. This waveform is processed through the time picking function, which results in an improved time of arrival. The implemented time picking functions are listed in appendix B, which has been taken from the exploratory work by Scheeren [23]. For implementation in the post-processing system the existing functions have been optimised with respect to their computational intensity.

Based on this improved time of arrival, and the waveform, a signal to noise ratio is determined using the following equation:

$$\mathrm{SNR} = 10\log_{10}\left(\frac{\sum U_{a+}^2}{\sum U_{a-}^2}\right) \tag{8.1}$$

In this equation the signal to noise ratio is determined by comparing the discrete energy before and after the determined time of arrival. U_{a+} indicates a series of samples following on the time of arrival, U_{a-} a series of samples preceding it. The number of samples within each series is imposed by the sampling rate and the selected signal to noise window. For this assessment the signal to noise window has been set to $T_{SNR} = 10\,\mu s$, to only evaluate the distinction of the signal and the noise around the onset of the acoustic wave.

The signal to noise ratio and the shape of the time picking processed waveform may subsequently be used to determine a logical value for time picking filtering. This value can be used in the localisation module to judge the validity of a time pick and the correlated event. For the theoretical study of this thesis the choice has been made to omit time picking filtering.

The final step in the time picking process is storing the selected times of arrival in the database.

Event Building. The second of the options is the event building module, driven by the function *fMasterEventBuilding.m*. Most of the structure of the event building module is similar to the time picking module; there are also three parts identifiable.

The first of these is used to obtain the time picking parameters. Four user defined parameters govern the time picking process. The database is checked for existing parameters, and when required new parameters are requested.

[2] A transient index, or a TRAI, is an integer assigned to an acoustic wave for cross-referencing data between the databases

The second part again is designed to select and obtain the starting point for the time picking process and to select the desired runtime. The options to continue or restart the process remain to be the two choices available. Continuing the event building process will start of at the first hit of the last existing event in the database, this means the last event is always recreated.

The process of event building is contained in the third part of the event building module. In itself it is also subdividable into three stages. The first stage divides all hits into groups, the so called events, based on the time difference of arrival of each couple of subsequent hits. The event separating criterion is the first hit channel discrimination time (FHCDT). The following logic is applied in this process:

$$t_{a_n} - t_{a_{n-1}} \begin{cases} \leq \text{FHCDT} & \rightarrow \quad \text{Hit } n \text{ in Current Event} \\ > \text{FHCDT} & \rightarrow \quad \text{Hit } n \text{ in New Event} \end{cases} \tag{8.2}$$

Besides the separation of hits into events, event building also serves to fine-tune these events with respect to their quality. The three other event building parameters are used for this process. Three logic filters are applied to decide whether an event remains "open" (1) or will be "closed" (0). A closed event will remain closed, a new event is required to reset to open. Hits arriving in the closed part of an event will not be used for further processing. Three criteria have been implemented to close events.

The first of these criteria is a check for duplicate channels within a single event. The process is governed by the user input AlDuChan, indicating the allowance or non-allowance of duplicate channels occurring within an event. This value is compared to occurance of duplicate channels to determine whether the hit is assigned a 1 or a 0. A 1 is assigned either if duplicate channels are allowed, or if no duplicate channels are present in case they are not allowed. A 0 is assigned if duplicate channels are present when these are not allowed.

The other two criteria are time-based criteria with a comparable means of processing to the FHCDT. These two criteria are the first hit maximum time difference (DT1Xm) and the previous hit maximum time difference (DTnXm). The applied logic for the first hit maximum time difference is given by:

$$t_{a_{E_n}} - t_{a_{E_1}} \begin{cases} \leq \text{DT1Xm} & \rightarrow \quad 1 \\ > \text{DT1Xm} & \rightarrow \quad 0 \end{cases} \tag{8.3}$$

In this equation the subscripts $E_{n/1}$ refer to the current and first hit within a specific event. The DT1Xm bounds this time, making it a sort of maximum event length criterion.

In contrast to this the logic for the previous hit maximum time difference is described as follows:

$$t_{a_{E_n}} - t_{a_{E_{n-1}}} \begin{cases} \leq \text{DTnXm} & \rightarrow \quad 1 \\ > \text{DTnXm} & \rightarrow \quad 0 \end{cases} \tag{8.4}$$

The subscripts $E_{n(-1)}$ now refer to the current and next hit within a single event. In this sense it is very similar to the process of first hit channel discrimination, though what sets it apart is the fact that it is only used to close events, not to create new ones. This makes it a means of fine-tuning within an event.

If all of the three criteria and the previous hit provide a value of 1 the hit will be assigned a 1 to indicate it as part of the open event. In case any of the four values provides a 0 the hit will be assigned a 0 to indicate it as a part of the closed event. When the considered hit is the first hit of a new event it will always be assigned a 1.

The final stage of event building writes the built events and the open-closed status to the database.

Receiver. The receiver module is used to specify the receiver grid. It is governed by the function *fMaster-Receiver.m*. This module provides four functionalities.

The first of these is to present a list of the properties of the receivers currently present in the secondary database.

However the main functionality of the module is to add receivers to the database. To achieve this three options have been included. The first is to manually add the channel number, coordinates and usage of each of the receivers. An alternative to this is to specify the channels, coordinates and usage in a structured Excel table, and to load this table into the database. The last option is to use a structured range table, and the receiver positioning algorithm developed by Scheeren in his exploratory work [23].

Additionally it is possible to alter specific receivers. Alteration of a receiver is aimed at changing a single property of this receiver at a time. This option may also be used to remove a single receiver from the database.

A final possibility is to remove all receiver data from the database.

Localisation. The last of the implemented modules contains the localisation functionalities. It is programmed in the file *fMasterLocalisation.m*. The localisation module follows a structure similar to the time picking and event building modules. It once again comprises of three steps.

The first step is to selecting the data set that needs processing and checking or specifying the speed of sound. For data set selection all time picking characteristic function couples present in the database are listed. Each of these is selectable, even if no earlier processing step has been initiated. Any missing data will lead to rejection of the event as valid for localisation. Therefore checking the status of a dataset prior to initialising localisation is advised. Additionally to data selection the selection or confirmation of a speed of sound is part of the first step in the module.

The second step is once again to select and obtain the starting point and to specify the desired runtime.

The third step covers the two stages of localisation. The first of these is validation. The validation process checks and matches the results of several other post-processing modules, and based on this determines if an event is valid for localisation. An important factor in this decision is the critical number of hits, which states the minimum amount of validated hits required within an event to consider it locatable. If an event is deemed valid an array of the valid hits of this event is stored in the database to be used for the actual process of localisation.

The second stage of localisation is localisation itself. For this process the system reads the list of validated hits, and subsequently acquires the associated times of arrival and receiver positions. This data is fed into the localisation solver.

Two alternatives to solve the localisation problem have been implemented. The primary of the two is programmed in the function *fPreDefMin3Dvolu.m*; which contains a MATLAB default multi-variable non-linear minimisation function to solve the LUCY problem presented in section 3.3. The alternative to this method is a planar localisation scheme, which binds the solution of the minimisation problem to a plane in $\mathbb{R}^3$. This function requires the formulation of a representative crack plane, which is dependent on the post-fracture geometry of the specimen. A skeleton code imposing a horizontal crack plane is implemented in the function *fPreDefMin3Dplan.m*.

The results of this solver are written to the database. Additionally a location filter may be implemented to systematically judge the quality of the obtained result. Since no feeling for actual localised AE fatigue crack data has been acquired no such filter is implemented.

8.4. Secondary Database

The post-processing system is designed around the principle of data storage. As such the secondary database, which stores this data, is an important aspect of the development of the post-processing system. This section elucidates the format, structure and contents of the secondary database.

The secondary database, like the primary and transient databases, will be stored in a binary format accessible through a structured query language (SQL). The specific format for this database, and those used by Vallen Systeme, is SQLite3, which is available in the public domain. To interface with the databases a MATLAB executable *mksqlite.mexw64* developed by Martin & Kortmann is used [17], which is available under the GNU Lesser General Public licence. This executable adds functionalities to MATLAB which allow it to access the binary database files and to process SQL command queries.

Using this format a database is created to store post-processed data. This secondary database contains six tables, as illustrated by figure 8.4.

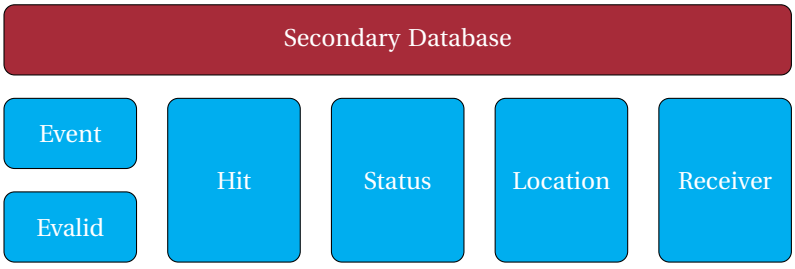

Figure 8.4: Overview of Secondary Database Contents

Status. The status table contains status data on the post-processing progress. It is structured around specific time picking characteristic function couples. For these couples it lists specified analysis parameters, such as the time picking options and discrimination times, and the speed of sound used for localisation. The table also contains a series of rows containing counters for time picking, event building, and localisation progress and validity.

The post-processing system uses the status table to keep track of the existing time picking characteristic function couples, and associated analysis parameters. The counters are solely used as a feedback mechanism to the user, and are not involved in determining starting points for start-stop operation.

Hit. The hit table contains post-processed hit data and is structured around the transient indices. For these transient indices it also provides the channel number, and when event built the number of the event it is associated with. For the time picking characteristic function couple specific data, such as the picked time of arrival, the table contains three more columns per existing couple. These columns contain the picked time of arrival, the signal to noise ratio associated with the recorded arrival time, and a logical value for a time picking filter.

Besides storage of time picked data, the hit table is used by the post-processing system to determine the starting point for the current hit when time picking of an existing couple is continued.

Event & Evalid. The event and evalid tables are supportive to event building. They contain rows of built events and columns of associated hits or the validity of these hits. A more elaborate explanation on the process of time picking is given with section 8.3.

The post-processing system uses the event table to determine the starting point for the current event and current hit when event building is continued. The evalid table is used in the validation process of event localisation.

Receiver. The receiver table contains a list of the channel numbers, three Cartesian coordinates and usage of the receivers that have been used to record the dataset. Three uses are recognised by the post-processing system. A receiver is either inactive (0), active (1) or active as a guard (2).

The receiver table is, obviously, used by the post-processing system in the localisation of events.

Location. The location table contains processed event data. It is structured around the event indices that have been generated during event building. Series of columns contain data related to a specific time picking characteristic function couple. Part of these columns are related to event validation; these store logical values to indicate valid events, and store arrays of valid hits related to that event. The rest of the columns associated with a specific time picking characteristic function couple contain the localised coordinates and the LUCY values, and provide the option to store logical values for a location filter as well.

The post-processing system uses the location table, again quite obviously, in the process of localising events. It is also where the crack propagation representation module will draw its input from.

9

Simulated Validation

This chapter elucidates the capabilities of the acoustic emission post-processing system by means of a simulated validation study. At first the methods of simulation and the design of the specimen are considered. These involve two approaches to investigating the accuracy. Subsequent to this the results of these two simulation approaches are evaluated and discussed. Based upon these results a set of boundary conditions will be drafted which guide the requirements for in-situ experiments.

The need for a simulated validation of the volumetric localisation system arose when, over the course of the project, experimental validation had shown to be unreliable. Appendices C and D, and the general and research introductions, provided in chapters 1 and 7, delve deeper into the experimental difficulties that have been faced. To mitigate adverse effects a simulated approach to system validation has been defined.

This validation comprises of two simulations aimed at disentangling the causes of either bias or variance. The first of these is aimed at uncovering the bias of a localised source for data with a minimal variance; it is focussed on mapping the bias and variance on the outer surface of the considered specimen. The second simulation is aimed at uncovering the development of the bias and variance in noisy conditions.

9.1. Methods of Simulation

The general approach to the simulated validation is similar to the one used in earlier exploratory work performed by Scheeren [23]. It uses the principle that an acoustic emission receiver comprises a piezoelectric transducer, which is inherently able to act as a receiver and a source [6]. The act of using a transducer as a source to emit elastic waves is generally referred to as pulsing. The advantage of source pulsing over applying Hsu-Nielsen sources[1] is in the repeatability of the process. Source pulsing allows for quick generation of large sample sizes with a high source location steadiness.

Steadiness of the source location is a desired quality for the simulations since it decreases the spreading of the source origin. This allows for a more distinct investigation of both the bias and the variance. Which, in turn, is critical for the considered level of scale.

However, steadiness of the source location will only deliver a clear look into the bias if the actual position of the source is known with very low tolerance. This will require a method to either accurately position or accurately measure the positions of the sources and receivers. For this study the issue is solved through receiver positioning by marking out transducer positions when milling the specimen. This is discussed more thoroughly with the design of the specimen.

Specimen Design

A specimen has been designed specifically to allow for high accuracy transducer placement for both receivers and sources. With respect to the design philosophy two variants have been considered. One which closely represents the geometry around an attachment of a tubular specimen, as a means to prepare for in-situ measurement. Another which is regularly shaped, and thus provides a more general insight into the accuracy. The latter has been chosen for the specific reason of obtaining more general knowledge.

[1] A Hsu-Nielsen source is a calibration procedure that is performed by breaking a pencil lead over a support shoe onto the object under consideration. Standards for Hsu-Nielsen sources are documented in ASTM E976

With this in mind a cube has been proposed for the design of the simulation specimen. It has been sized 100 by 100 by 100 millimetres. Which means it has a relatively large size compared to the scale of the accuracy under investigation. The purpose of this is to allow for a larger working area. A larger working area ensures that a more complex source pattern can be imposed, which will provide more elaborate knowledge on the differences in the accuracy in space. The source pattern is discussed in more detail further on in this section. First the fabrication and the properties of the cube are discussed.

Figure 9.1: Instrumented Cube Specimen
Visible are the top, side and front faces

Fabrication & Properties. The cube, which is depicted in figure 9.1, has been milled out of a solid block of aluminium. For this process a five-axis machining centre has been used, which guarantees a tolerance of 0.01 mm. Sensor positions for both sources and receivers have been marked out as circular indentations optimised for VS600-Z2 transducers. As such the indentations have a diameter of 5.00 mm and a depth of 0.10 mm. The coordinates of the centres of each of the indentations are presented in tables 9.3 and 9.2 relative to the centre of the cube.

The receiver indentations are slightly oversized compared to the listed diameter of the VS600-Z2 transducers [33]. This has been implemented to allow for some tolerance in the exact transducer geometry and for the flow of the coupling agent. Though this also imposes a slight uncertainty on the exact placement of a transducer. The in-plane axial difference between the table listed centres, measured or ^{M}, and the actual transducer positions, true or ^{T}, could differ up to 0.125 mm. This can be expressed as:

$$R^T = R^M + \varepsilon_p \tag{9.1}$$

And:

$$S^T = S^M + \varepsilon_p \tag{9.2}$$

Here ε_p represents the in-plane transducer placement error of up to 0.125 mm radially.

The choice to produce the cube out of aluminium has been made based on both weight and cost. The same specimen in steel could weigh up to trice as much at nine times the material cost. Handle-ability of the cube was an important factor to its design. However the acoustic qualities of the cube may differ from the steel tubular and bar specimen, because the material properties of aluminium differ from those of steel.

A difference in the material properties typically implies to a difference in the speed of sound. This difference in the speed of sound is a critical parameter in the comparability of the results for steel and aluminium specimen, since it influences the localisation resolution. An estimation of the speed of sound for a dilatational plane wave can be made using the following equation [19]:

$$V_1 = \sqrt{\frac{3K}{\rho} \cdot \frac{1-\nu}{1+\nu}} \tag{9.3}$$

This equation shows that the speed of sound is dependent on the bulk modulus, the density and the Poisson ratio; represented in the equation by K, ρ and ν respectively.

These material properties are listed in table 9.1, where the range of their values for aluminium is also given. Additionally the calculated range for speed of sound is also presented in this table. This range contains the plane wave velocity of steel ($V_{1,S} = 5950\ ^{mm}/_{ms}$), which makes aluminium an acceptable substitute for steel with respect to the acoustic properties. A calibration procedure will determine the exact speed of sound of the cube specimen.

Table 9.1: Several Material Properties of Aluminium [14]

Parameter	**Symbol**	**Value**	**Unit**
Bulk Modulus	K_{Al}	$64-69$	GPa
Density	ρ_{Al}	$2.5-2.9$	$^{Mg}/_{m^3}$
Poisson Ratio	ν_{Al}	$0.32-0.36$	–
Volumetric Velocity	$V_{1,Al}$	$5581.8-6531.0$	$^{mm}/_{ms}$

Receiver Configuration. The front and aft faces of the cube have been marked for receiver positions. These receivers span a rectangular grid composed of eight corner points. Four of these points are present on the aft face, these are also indicated in figure 9.2 by the R-preceded channel numbers. The other four are present on the front face, and similarly shown in figure 9.5. Table 9.2 lists the centres of the receiver indentations.

Table 9.2: Cube Specimen Receiver Positions

Channel	***X*** $[mm]$	***Y*** $[mm]$	***Z*** $[mm]$	**Usage**	**Face**
1	−50.00	40.00	40.00	Active	Aft
2	−50.00	40.00	−40.00	Active	Aft
3	−50.00	−40.00	40.00	Active	Aft
4	−50.00	−40.00	−40.00	Active	Aft
5	50.00	40.00	40.00	Active	Front
6	50.00	40.00	−40.00	Active	Front
7	50.00	−40.00	40.00	Active	Front
8	50.00	−40.00	−40.00	Active	Front

Source Positions. Four of the faces of the cube have been marked with nine source positions each, for a total of 39 source positions. These positions have been designed in a grid for one of the faces, and subsequently been rotated by 30°, 60° or 90° for each of the other faces. Table 9.3 lists the centre of each source indentation. The face and order refer to figures 9.2 through 9.5, which graphically display the positions of each source indentation. The side face has been marked with the designed non-rotated source grid.

Table 9.3: Cube Specimen Source Positions

Face	Order	X $[mm]$	Y $[mm]$	Z $[mm]$
	1	−50.00	0.00	0.00
	2	−50.00	15.00	25.98
	3	−50.00	3.84	26.65
	4	−50.00	−25.98	15.00
4 | Aft	5	−50.00	−11.83	−10.49
	6	−50.00	−10.00	−17.32
	7	−50.00	20.31	−34.82
	8	−50.00	17.32	−10.00
	9	−50.00	22.32	−1.34
	1	0.00	0.00	50.00
	2	−17.32	10.00	50.00
	3	−12.32	18.66	50.00
	4	15.00	25.98	50.00
1 | Top	5	21.16	16.65	50.00
	6	25.98	−15.00	50.00
	7	−3.17	−15.49	50.00
	8	−10.00	−17.32	50.00
	9	−40.31	0.18	50.00
	1	0.00	−50.00	0.00
	2	−15.00	−50.00	−5.00
	3	−20.00	−50.00	0.00
	4	−20.00	−50.00	35.00
2 | Side	5	0.00	−50.00	20.00
	6	10.00	−50.00	20.00
	7	30.00	−50.00	0.00
	8	25.00	−50.00	−10.00
	9	0.00	−50.00	−30.00
	1	50.00	0.00	0.00
	2	50.00	−5.00	15.00
	3	50.00	0.00	20.00
	4	50.00	35.00	20.00
3 | Front	5	50.00	20.00	0.00
	6	50.00	20.00	−10.00
	7	50.00	0.00	−30.00
	8	50.00	−10.00	−25.00
	9	50.00	−30.00	0.00

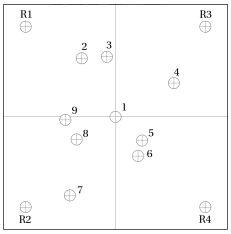

Figure 9.2: Source Positions on Cube Aft Face

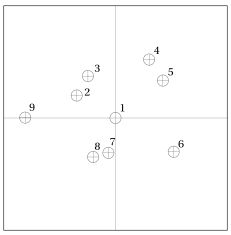

Figure 9.3: Source Positions on Cube Top Face

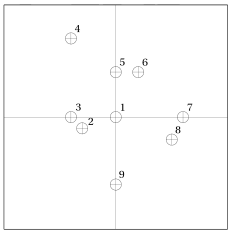

Figure 9.4: Source Positions on Cube Side Face

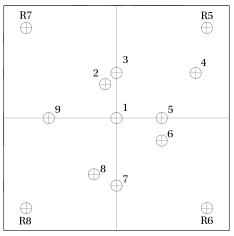

Figure 9.5: Source Positions on Cube Front Face

Ideal Conditions

A first measurement set is simulated and recorded while imposing ideal conditions on the specimen. The intent of this data set is to obtain a clear mapping of the ideal bias and associated minimal variance in a case of undisturbed accuracy. This data will provide a starting point for further evaluation of the accuracy development in disturbed conditions.

For this data set a VS600-Z1 receiver is used as a source. It is used to generate at least 100 events per source location, amounting to a total of at least 3,900 events. Because of the high amount of source location the choice has been made to omit the process of gluing the sources, with the intent of saving time on the duration of the data acquisition. Instead the source is connected to the cube through a petroleum-based coupling agent and manually applied pressure. Each of the source positions has been cycled through following increasing face and order numbers as listed in table 9.3.

Noise Evaluation

A second measurement set is simulated and recorded while imposing a varying range of noise and signal amplitudes on the specimen. The aim of this dataset is to investigate the effects of the signal to noise ratio on the bias and on the variance.

Similar to the no-noise set a VS600-Z1 receiver is used as a source for acoustic events. Noise is applied through a VS900-M broadband receiver connected to the remaining unmarked side face of the cube. To generate noise a Agilent 33500B-series function generator set to output Gaussian noise has been used. A test matrix has been defined based on the peak amplitudes of the signal and noise, which is presented in table 9.4. The values in this table describe the peak to peak ratios of the signal and the noise; as such it is an amplitude based ratio, in contrast to the SNR which is an energy based ratio. For each calculated ratio the lower limit of the signal peak amplitude range has been used.

Table 9.4: Signal and Noise of Test Matrix
Signal to noise ratio in decibel
N | Added Noise Peak Amplitude $[dB_{AE}]$
S | Signal Peak Amplitude Range $[dB_{AE}]$
X | No Value Determined

N / S	No	30	36	42	48	54	60
68/61	X	31	25	19	13	7	1
74/67	X	37	31	25	19	13	7
80/72	X	42	36	30	24	18	12
86/78	X	48	42	36	30	24	18
92/83	X	53	47	41	35	29	23

The simulation has been tuned for a source located at order 5 of the top face. Only a single location will be evaluated for all of the 35 signal to noise couples. A set of at least 100 events is generated for each of these. This amounts to a total of 3,500 events. Because of the extensive sample size for a single location the source will be glued to the cube. This assures a consistent coupling over the whole data set.

Subsequent to simulating the data set the actual energy based signal to noise ratio will be calculated for each hit. The time-picked onset of the acoustic wave is used as the separating criterion for noise and signal. The minimal SNR within an event will be used as normative to that event. To determine the energy based signal to noise ratio equation 8.1 is used.

9.2. Calibration

In order to obtain obtain the best results after post-processing an extensive calibration campaign is performed. This campaign is focussed on obtaining a complete understanding of the speed of sound and the possible irregularities in the specimen or receiver grid. To this purpose eight paths have been defined for which pencil lead breaks are performed. To keep the total amount of breaks to a reasonable number each of the paths is excited by five Hsu-Nielsen sources. An overview of the paths, average time differences of arrival and average speeds of sound is given in table 9.5.

This table presents the speed of sound for three time picking methods, applied to three types of characteristic functions[2]. For threshold-based time of arrival selection the time differences of arrival have also been included. All values in the table have been averaged over the sample of Hsu-Nielsen sources excited along that path. At the bottom of the table the averages of all speeds of sound are determined per time picking characteristic function couple.

To start with the threshold based values. Most of the time differences of arrival presented in this column show values between $12.60 \leq t_\delta \leq 12.70$ µs. However, those related to channel 6 come closer to 12.80 µs. This might be an indication of an error in the placement or coupling of the receiver associated with channel 6, though it may also be related to the problem associated with threshold time picking. This observation was the main instigator to inspect each path more closely through other method of time picking, opposed to only considering the average of the whole in the context of time picking.

[2]Characteristic functions are waveform envelope functions applied to the input of time picking functions to improve sensitivity.

When the time-picked speeds of sound are observed the assumption that channel 6 might induce a dissimilarity in the measurement does not hold, as it does not necessarily show up as an extreme. In general the time-picked speeds of sound show a lower range of speeds of sound over the different paths, and a higher speed of sound. The higher speed of sound is likely the result of the sensitivity to attenuation of the threshold based picking method. In the analysis of results each of the sets of time-picked data will be evaluated based on their individual speed of sound.

Table 9.5: Cube Specimen Speed of Sound Calibration
AIC1 | Single Pass AIC picker – 200 µs window of first pass
AIC2 | Double Pass AIC picker – 25 µs window of second pass
Allen | Characteristic function by Allen [2]: $y_i = x_i^2 + k\left(x_i - x_{i-1}\right)^2$
Abs | Characteristic function by absolute value: $y_i = |x_i|$
No | No characteristic function: $y_i = x_i$

	Threshold		AIC1			AIC2		
			Allen	Abs	No	Allen	Abs	No
Path	t_δ [μs]	c [$^{mm}/_{ms}$]	c [$^{mm}/_{ms}$]	c [$^{mm}/_{ms}$]	c [$^{mm}/_{ms}$]	c [$^{mm}/_{ms}$]	c [$^{mm}/_{ms}$]	c [$^{mm}/_{ms}$]
1–2	12.65	6324.1	6317.9	6315.4	6315.4	6315.4	6317.9	6314.1
3–4	12.66	6319.1	6392.3	6394.9	6389.8	6397.4	6389.8	6392.3
5–6	12.86	6220.8	6314.1	6309.1	6309.1	6314.1	6306.7	6304.2
7–8	12.60	6349.2	6259.8	6392.3	6405.1	6394.9	6410.3	6402.6
3–1	12.70	6299.2	6346.7	6349.2	6346.7	6346.7	6344.2	6346.7
4–2	12.70	6299.2	6364.4	6364.4	6366.9	6364.4	6366.9	6361.8
7–5	12.62	6302.0	6415.4	6410.3	6412.8	6397.4	6402.6	6392.3
8–6	12.80	6250.0	6324.1	6334.1	6329.1	6324.1	6329.1	6324.1
Average		6295.5	6341.8	6358.7	6359.4	6356.8	6358.4	6354.8
$\mathbf{max}(c) - \mathbf{min}(c)$		128.4	155.6	101.1	103.7	83.3	103.6	98.4

Table 9.6: Considered Sample Size per Source Location
F | Face
O | Order

O \ F	4 | Aft	1 | Top	2 | Side	3 | Front
1	102	104	104	103
2	64	107	103	104
3	94	100	106	100
4	14	103	103	25
5	102	101	104	102
6	108	104	103	102
7	90	103	103	105
8	101	102	103	103
9	101	104	104	98

9.3. Undisturbed Accuracy

By applying the methods described in section 9.1 under "Ideal Conditions" a dataset has been generated. This dataset has been analysed to investigate the source location dependency of the accuracy parameters. For this dataset time picking was performed using AIC1 with no characteristic function. For localisation a speed of sound of $c = 6359.4$ $^{mm}/_{ms}$ has been specified.

During the processing of the localised results a LUCY filter was applied to remove estimated source locations with a hight uncertainty. This filter has been set as a low-pass-cut-off for LUCY ≤ 1 mm. A result of this decision is that not all source locations still provide an evaluated sample size of more than 100 events. An

overview of the sample size for each of the source locations is presented in table 9.6. This table shows that for some of the source locations on the front and aft face a significant amount of source estimations were deemed uncertain. On the side and top face all source estimations passed the filter. This may be a precursor of the relation in the accuracy between the top and side, and front and aft faces.

For the analysis of the undisturbed accuracy a bottom-up approach is used. As such the variance and bias are discussed first, followed by the MSE.

Variance

For each of the source locations the variance of the sample of source estimations has been calculated. This variance composes of the variance along each of the Cartesian axes, and a combined variance based on the principle of independence, i.e. the sum of the components. For each of the investigated faces a plot is made to compare the components of the variance.

Results obtained for the top face are presented in figure 9.6. This figure is flanked by figure 9.7, which displays the side face. These two figures are presented side-by-side because they show very similar results. Their comparability becomes especially evident when one notices that the top face is characterised by bordering the outermost Z-dimension, with XY as the in-plane dimensions, and that the side face is characterised by bordering the outermost Y-dimension, with XZ as the in-plane dimensions. The top and side faces are essentially Z-Y-transformed versions of each other.

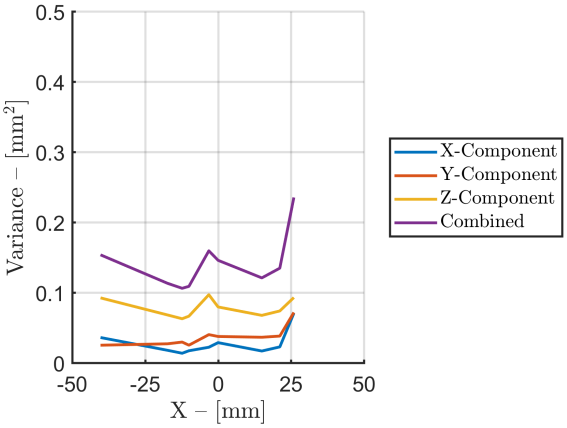

Figure 9.6: Variance on Top Face against X-direction

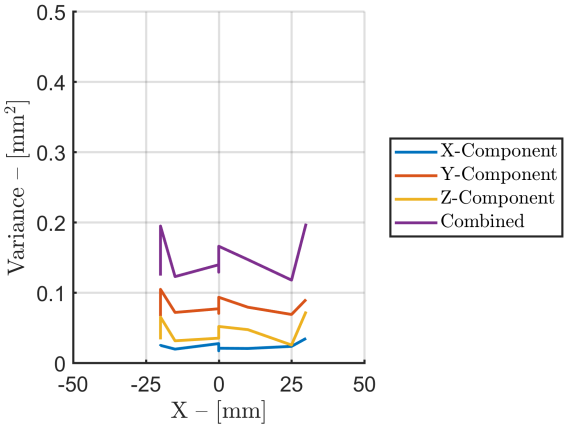

Figure 9.7: Variance on Side Face against X-direction

Both of the faces show an in-plane variance where both of the Cartesian axes are comparable to each other. There seems to be no specific dependency of the variance on the in-plane source location. A rather conservative limit for this single-dimensional in plane variance would be Var = 0.05 mm^2, this amounts to a 99% confidence interval on the single-dimensional cluster size of $6\sigma = 1.34$ mm.

The out-of-plane direction shows a clear increase of the variance, as would be expected for a plane that borders the edge of a receiver grid. Both the variances along the Z-direction for the top face and the Y-direction for the side face display an upper limit of about Var = 0.1 mm^2, twice that of the in-plane directions. As such the cluster size along the out-of-plane direction becomes $6\sigma = 1.90$ mm.

If the variance on each of the axes is deemed to be independent of one another, then the combined variance is equal to the sum of the variances. This value is also included in the presented graphs. Summing the described upper limits for the in- and out-of-plane variances results in a upper limit of $\text{Var}_c = 0.2$ mm^2. The graphs in figures 9.6 and 9.7 show this limit is surpassed once, and approached twice. A slightly less conservative limit, which still represents 83% of the data would be $\text{Var}_c = 0.15$ mm^2. The diameter of the cluster encompassing 99% of the samples of these 83% of the locations would be $6\sigma_c = 2.32$ mm.

These presented results seem to paint a bleak image of the obtainable precision, which contrasts to the results of the exploratory study. However, if several parameters related to a fair comparison are taken into account the results are no longer surprising. In the exploratory work one of the AIC time pickers achieved an precision of $6\sigma_x = 0.917$ mm [23]. Assuming independence of each of the axes, which is a conservative assumption, a theoretically obtainable three-dimensional combined variance would be equal to $6\sqrt{3}\sigma_x = 1.588$ mm. Though this does not yet take the geometric delusion of precision into account, which amounts to a

single-dimensional factor of 2 in the variance when a location at the centre is compared to one at the border of a receiver grid [30]. Including this prescribes a theoretical variance at the border equal to $6\sqrt{6}\sigma_x = 6\sigma_c \approx 2.246$ mm, which is in line with the results presented for the top and side faces.

The results obtained for the front and aft faces should provide a comparable similarity. Therefore these are also shown side-by-side in figures 9.8 and 9.9 respectively. Three clear observations can be made for these two figures. The first is that they indeed depict a similar trend in the variance. There are some peaks and troughs present in either graph, through the general range of most of the values is comparable. The other two observations are made in relation to the graphs for the top and side faces. The front and aft faces show a much more irregular distribution of the variance along their respective horizontal axis in comparison to the top and side faces, and additionally the value of the variance for the front and aft faces seems generally higher for all of the components.

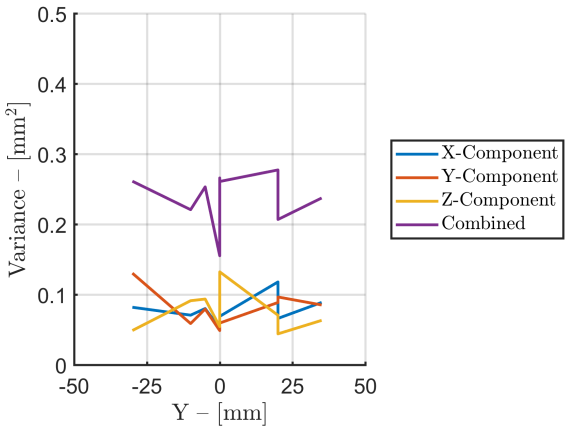

Figure 9.8: Variance on Front Face against Y-direction

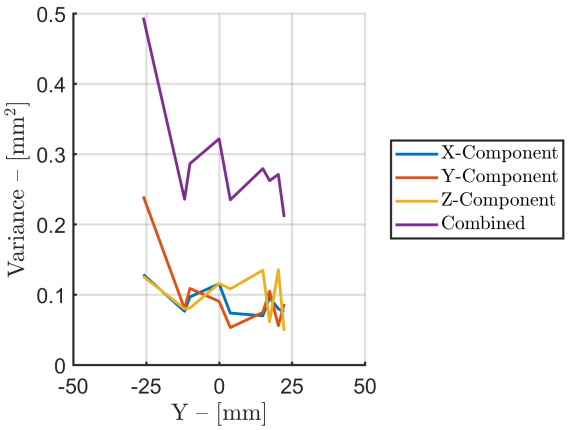

Figure 9.9: Variance on Aft Face against Y-direction

These observations seem to indicate that the variance on the front and aft faces is worse in both value and predictability than the variance on the top and side faces. A possible explanation for the lower precision may be interference caused by the other source indentations on the same measurement plane. Since the front and aft faces also had the receivers installed on them. In most cases at least one path from any source to the four receivers on that face is obstructed by another source indentation. The one source that has a clear path to all of the four receivers on the same face is order 1 on the front face. The combined variance for this source position also shows a significant drop, indicating a higher precision. The value for this source corresponds to the order 1 values for the top and side faces. This single case backs up the assumption that the other source indentations deteriorate the localisation precision, though cannot serve as a proof of this on its own.

Bias

For each of the source locations the bias of the sample of source estimations has been calculated. This bias composes of one component along each of the Cartesian axes. For each of the axial components of the bias an individual plot made to correlate the bias on multiple faces.

The first of these plots is presented in figure 9.10, which shows the dependency of the X-component of the bias on the X-coordinate. For the top and side faces there seems to be a slight linear trend in the bias, which additionally seems to be shifted towards a positive bias. This trend is minimal and only accounts for a shift of up to a millimetre over a length of 50 mm.

Much more significant is the X-component of the bias on the front and aft faces. These show a bias that opposes the direction of the linear trend visible for the other faces. This is quite a surprising result, for which there is no mathematical basis in the solution to the localisation problem. Therefore it may be a wave propagation issue, related to the source and the receivers being on the same surface. This statement may be confirmed by the other bias components. What is important to note in this case, is that the X-component of the bias is strongly dependent on the time of arrival differences between the front and aft face. This wave propagation problem would introduce a slight delay on the arrival at the receivers on the source face, accounting for a inward-shift of the localised sources.

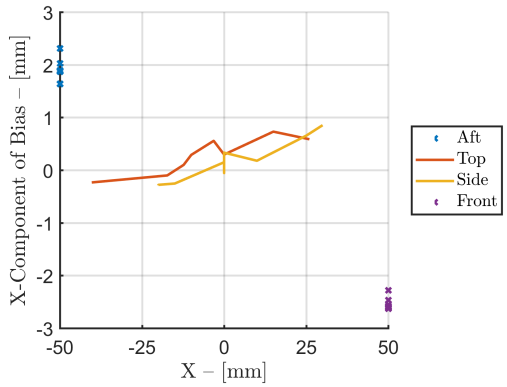

Figure 9.10: X-Component of Bias against X-direction

The other two components of the bias, those along the Y- and Z-directions, depicted in figures 9.11 and 9.12 respectively, show a much stronger dependency on their respective Y- and Z-coordinates. Additionally to a stronger dependency of the bias on the position they also show a very clear similarity to each other. The positive trend in the bias development, which seems to favour an outward-shift of the localised sources, is visible on all three directional components of the bias. This indicates that it is related to a similar cause, which is most likely an overestimated speed of sound.

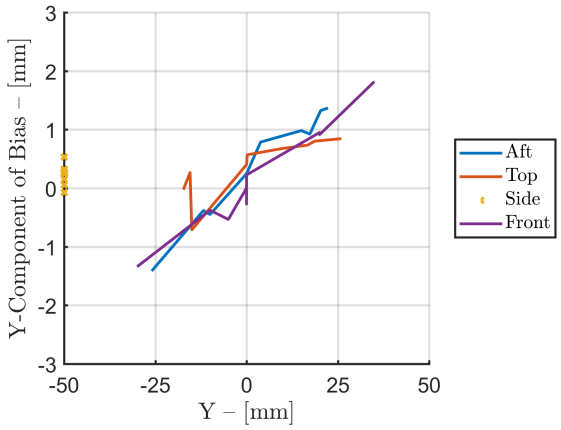

Figure 9.11: Y-Component of Bias against Y-direction

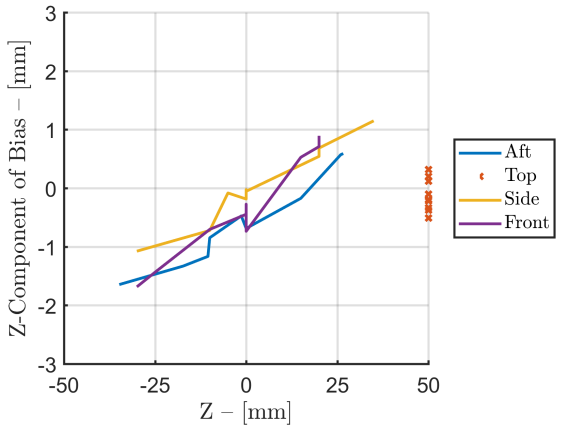

Figure 9.12: Z-Component of Bias against Z-direction

Another thing that is quite surprising in the graphs of the Y- and Z-components of the bias is that the perpendicular faces to these Cartesian axes show a rather low, nearly insignificant, bias. It is unclear what causes this effect, but it is expected to be unrelated to the anomaly experienced with the front and aft faces of the X-component of the bias.

An observation in relation to this X-component of the bias is that the top and aft faces do correspond to the general trend on the other faces of the Y and Z bias components. Which would be expected with regards to the assumed origin of the anomaly in the X-component. And what must be kept in mind with this is that these to components depend on the top and bottom, and right and left side time of arrival differences. Under the assumption that propagation is corrupted if a source and receiver are on the same face, this all adds up to a positive conclusion. If a whole receiver face, and only one of the two receiver faces, gets corrupted equally, the in-plane solution remains the same, only the out-of-plane solution deteriorates. Which is exactly what the results show. The question that remains is what is causing this propagation delay on the receiver-source face. The most likely answer is the transducer indentations. These likely have an effect on the wave propagation along the face.

To verify the assumption that an overestimation of the speed of sound accounts for the profile of the bias presented in figure 9.10 through 9.12, a numerical simulation is performed. This simulation evaluates a two-dimensional situation where four receivers span a square centred around the origin. Sources are imposed from the origin outward along a line perpendicular to the border of the receiver box. A speed of sound com-

parable to that in the cube is used to determine the simulated TOA's. A deviation of 5% or 10% is imposed on the speed of sound used in the localisation scheme. The bias along the direction of the imposed source line is considered. Results are presented in figure 9.13.

From this figure one can conclude that the assumption that a overestimation of the bias accounts for an outward-shift of the localised sources is correct. This also implies that a downwards correction of the speed of sound may be utilised to reduce this bias.

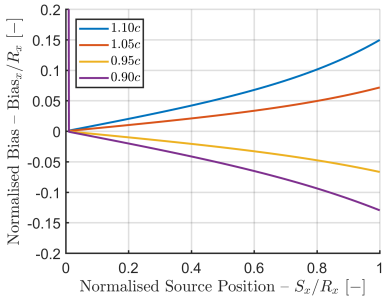

Figure 9.13: Speed of Sound Induced Bias Relative to Source Position

To conclude on the evaluation of the bias a plot has been made of the combined bias, which is prescribed as the Pythagorean sum of the bias components. This plot is depicted in figure 9.14, and to give a fairer comparison to a combined parameter, has been plotted against the radial distance from a source to the centre of that face. It shows that the absolute bias closer to the centre of the face is dominated by the bias component perpendicular to that face, and that a slight increase starts to appear as the sources move outward.

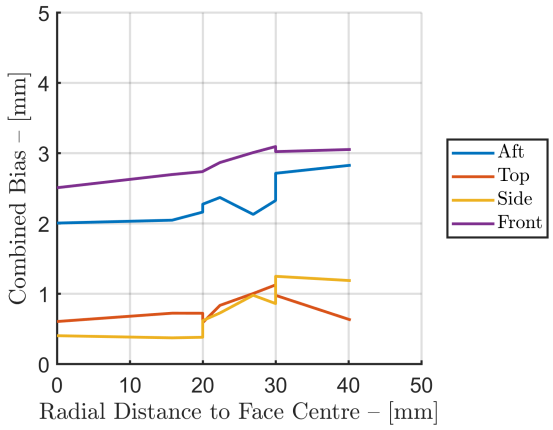

Figure 9.14: Combined Bias against Radial Distance to Face Centre

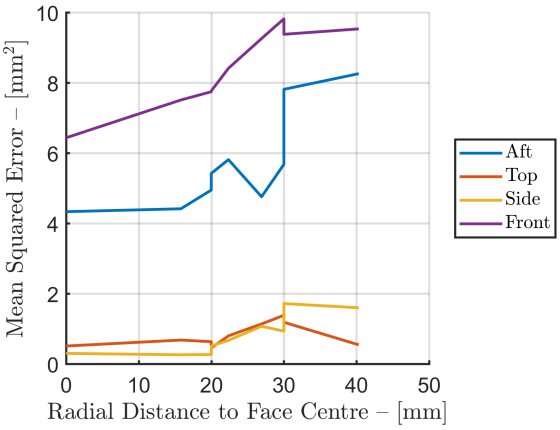

Figure 9.15: MSE against Radial Distance to Face Centre

Mean Squared Error

And finally the mean squared error is considered. Like the combined bias it is plotted against the radial difference from the centre of a face, to give a fairer comparison of a combined parameter. The resulting plot can be found in figure 9.15. It shows a graph that mostly seems like a squared version of the combined bias graph of figure 9.14. This was to be expected since the MSE is equal to the sum of the variance and the squared bias. Since the latter of these two is generally of a greater magnitude, it is dominantly present in the MSE. Therefore it shows the same trend as, and as such the same observations can be made as for, the combined bias.

9.4. Noise Sensitivity

By applying the methods described in section 9.1 under "Noise Evaluation" a dataset has been generated. This dataset has been analysed to investigate the signal to noise ratio dependency of the accuracy parameters. For this dataset all of the six time picking characteristic function couples were used as specified in table 9.5,

in order to compare the sensitivity to noise of each of the combinations. For localisation the associated speed of sound for each couple has been specified.

During the processing of the localised results no LUCY filter was applied. An overview of the sample size for each SNR is presented in table 9.7.

For the analysis of the noise sensitivity a top-down approach is used. As such the MSE is discussed first, followed by the variance and bias.

Table 9.7: Considered Sample Size per SNR
N | Added Noise Peak Amplitude $[dB_{AE}]$
S | Signal Peak Amplitude Range $[dB_{AE}]$

N / S	No	30	36	42	48	54	60
68/61	104	104	104	108	112	112	103
74/67	103	102	102	103	103	103	103
80/72	102	103	103	103	103	103	103
86/78	102	103	103	103	103	103	105
92/83	103	102	102	103	102	103	110

Mean Squared Error

The fist step in the evaluation of the noise sensitivity is to investigate whether the response to a certain signal to noise ratio is dependent or independent of the reference signal peak amplitude. To this purpose a plot has been made where the test matrix is broken up into separate signal peak amplitude ranges. This plot is shown in figure 9.16.

This figure shows that there is no clear distinction in the performance between an SNR obtained from a high amplitude signal with high amplitude noise, and one obtained from a low amplitude signal with low amplitude noise. Both of these lead to comparable accuracy, if the SNR is of the same magnitude. As such is is possible to combine the whole test matrix into a single SNR trace.

These combined test matrix SNR traces for the mean squared error for all of the six time picking characteristic function couples are presented in figure 9.17. This figure very clearly shows that there is a clear difference in the sensitivity to noise for the different time pickers, though not for the different characteristic functions. In the low noise ranges, SNR ≥ 30 dB, there does not seem to be a notable difference between either time picking function. However, as the noise increases the AIC2 picker starts to separate into a much steeper degradation of the accuracy with decreasing SNR. For the high noise range, SNR ≤ 20 dB, the MSE of the AIC2 combinations seems to reach a limit. The AIC1 couples catches up with this MSE limit after a steep increase of the MSE around $SNR = 10$ dB.

The crux of the noise sensitivity analysis is now to see in which ratio the precision and trueness make up for this accuracy. This will provide a basis to draft boundary conditions.

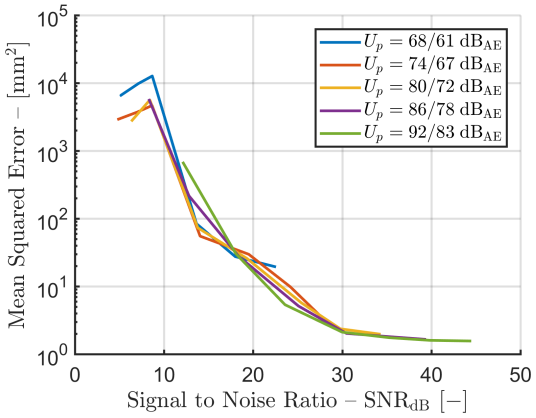

Figure 9.16: Peak Amplitude Separated SNR Evaluation of Combined MSE for AIC1|No

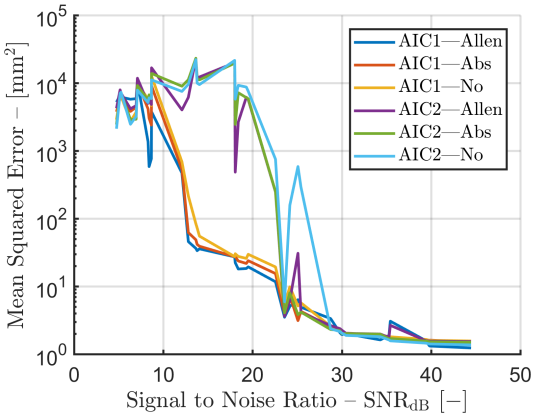

Figure 9.17: SNR Evaluation of MSE

Variance & Bias

In order to correctly disentangle the influence of both the variance and the bias on the MSE, they are presented side-by-side. Figure 9.18 displays the noise sensitivity of the variance, figure 9.19 the noise sensitivity of the bias. It is important to keep in mind that the bias is squared in the definition of the MSE.

While taking this into consideration it becomes clear that for a signal to noise ratio higher than SNR ≥ 30 dB the bias is the main contributor to the MSE. For a lower SNR the variance quickly catches up with the bias, and they remain of equal importance to the high noise accuracy.

In relation to this the bias seems to show a rather flat profile in the low noise area. It seems to start rising slowly for lower ratios starting at SNR ≤ 30 dB. However the variance seems to be much less flat in the low noise range.

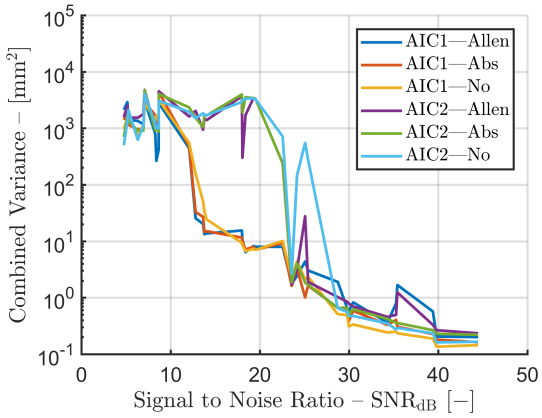

Figure 9.18: SNR Evaluation of Combined Variance

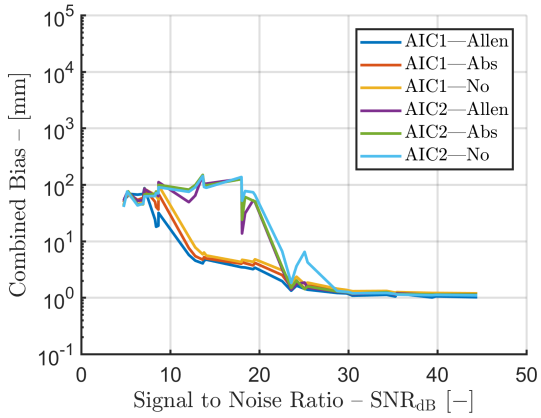

Figure 9.19: SNR Evaluation of Combined Bias

9.5. Boundary Conditions

To conclude upon the simulation part of this study a set of boundary conditions are drafted which are necessary for accurate source localisation. These are aimed at implementation for fatigue crack propagation monitoring. The goal of this implementation would be an accurate representation of the crack front. In order to achieve this one must note that:

A crack front is not localised by a single source. Multiple sources along the crack front need to be localised in order to correctly estimate the position of this crack front. As such the crack front estimation problem is a regression problem, with the localised sources as the input data. This means a regression function must be developed to obtain the crack front from the localised sources.

As a regression problem a slight variance in the data is of no concern as long as it is a consistent variance. The simulated mapping showed that the variance is largely consistent in between the receivers. On the edges a geometric delusion of precision occurs, which deteriorates the precision. Since this is an easily mappable mathematical property of the receiver array geometry, this is deemed to be no problem, and could be taken into account with the regression model. The only thing to worry about is to keep the variance within reasonable limits to perform decent regression. As such a signal to noise ratio above SNR ≥ 30 dB is required.

A more critical parameter to the regression problem is the bias. In general the bias should be as low as possible, since it directly influences the regressed position of the crack front. Taking the results of the simulation into consideration limits an acceptable bias to SNR ≥ 30 dB, which is the range where the bias remains stable, and mostly unaltered. In order to minimise the initial bias the receiver positions and speed of sound must be determined very accurately. It is proposed to develop an integrated method for positioning and speed of sound estimation based on receiver position pulsing.

10

Conclusion

This research project aspired to develop a volumetric acoustic emission fatigue crack monitoring system and to establish the limiting boundary conditions under which the system is capable of localising volumetric sources with millimetre accuracy. The previous two chapters have extensively covered the development of this system, and the procedure for establishing the limiting boundary conditions.

On the topic of system development the starting point has been defined by means of analysing the AMSY-6 acoustic emission measurement system developed by Vallen Systeme. Subsequently the requirements for the post-processing system have been defined, which were to lead to a system capable of performing up to par with the set goal. These requirements have been implemented in MATLAB, in a text based format. At the core of the post-processing system lies the secondary database, which assures preservation of the processed data.

Subsequent to the development of the system a validation campaign has been performed. This campaign was intended to utilise the tubular and bar experiments form the 4D-fatigue project, though these were deemed unsuccessful. Therefore a simulated approach was adopted. As such a cube was designed to assess the bias and variance in three dimensions. Additionally a noise sensitivity study was performed. These studies have shown that:

The consistency of the variance depends greatly on the face under consideration. For the top and side faces consistent results can be obtained. On the front and aft faces source indentations deteriorate the measurement.

The variance on the top and side faces is of similar magnitude to the variance obtained during the exploratory study, when comparing the AIC1 time picker. In the centre this is likely to allow for a single dimensional cluster no larger than $6\sigma = 1.34$ mm in low noise conditions. Along the edges of the receiver grid this variance is expected to increase to about $6\sigma = 1.90$ mm.

The bias, in case the receiver position have been established accurately, partly shows a trend that can be attributed to a difference between the imposed and actual speed of sound. This may be corrected through careful calibration. Another effect is in play on the bias perpendicular to a plane. These components shows an unexplainable low bias. Further research is required to gain an understanding of the causes.

The bias is a dominant factor in the calculation of the MSE. Similarly it influences the accuracy of the crack front estimation the most. Regression allows for obtaining a decent result from a cloud of points, however a shift of this cloud is not easily corrected without knowledge on the exact shift pattern.

Both accuracy parameters are sensitive to a signal to noise ration lower than $SNR \leq 30$ dB. The two considered time pickers show comparable results for this range of signal to noise ratios. At higher noise levels the AIC1 picker outperforms the AIC2 picker. Characteristic functions only add to the details. No characteristic function seems to perform better for the variance, while the function by Allen seems to perform better for the bias.

These observations lead to a set of boundary conditions regarding volumetric crack propagation monitoring that need to be considerd. As a first a large amount of hits is required to perform decent regression. Secondarily the bias must be kept to a minimum by accurately knowing the receiver geometry and the speed of sound. And finally the noise must be kept low, ideally under $SNR \geq 30$ dB, to warrant a decent bias and variance.

III

Reflection

11

Conclusion

At the start of this thesis the goal was set to develop a volumetric acoustic emission fatigue crack monitoring system and to establish the limiting boundary conditions under which the system is capable of localising volumetric sources with millimetre accuracy. However, maybe just as important is the observation made later in this same chapter that this thesis is a work of learning. Keeping both of these goals in mind the affiliation of this thesis with the established literature and research questions is assessed.

The first of the literature questions was; which current generation inspection methods are used to monitor fatigue crack growth? The study of the fundamentals of fatigue established that beach marks are typically inspected a posteriori to determine the crack growth rate. This method is unavailable for multi-axial fatigue due to the combination of tensile and shear modes, which may result in polishing of the beach marks.

The second of the literature questions was; what are the current day applications of acoustic emission methods for structural health monitoring? With the state of the art analysis it was established that feature analysis is typically used for growth rate analysis, and that localisation is typically used for global monitoring of a structure. However, some studies have also attempted to localise sources in small scale volumes during fracture events.

The third and final literature question was; which knowledge gaps exist in the combined state of the art of these fields? The literature study establishes that valuable knowledge may be gained by attempting to apply an approach similar to that of Ronde et alii for the purpose of volumetric localisation in small scale steel specimen. This study is to specifically aim at investigating the accuracy, in the form of variance and bias, that may be obtained.

Regarding the research task another for questions have been defined. The first of these was; which methods can be utilised to improve automated processing of acoustic emission localisation? This question is mostly covered in the development of the post processing system, which resulted in a system that has been used for the rest of the research presented in this document. A feature that not, yet, made it into the system was novel time-frequency onset detection, due to the computational intensity.

The second of the research questions was; what is the influence of a volumetric geometry on acoustic emission localisation? The study showed that, without noise, the results regarding the precision in a volumetric situation compare well to those established in an exploratory study on a plate. For the considered AIC time picker this precision comes close to a 99% confidence cluster of about a millimetre in size. Regarding the bias on the surface the study showed that accurate receiver placement and speed of sound calibration minimises the bias to a negligible trend in relation to the level of scale.

The third of the research questions was; what is the influence of noise on volumetric acoustic emission localisation? The noise sensitivity analysis showed that accurate source localisation is rather sensitive to noise. A signal to noise ratio of at least $SNR \geq 30$ dB is advised to obtain decent results, since up to this ratio the bias remains constant.

The fourth and final research question was; which boundary conditions must be met to accurately localise volumetric acoustic emission sources? The answer to this question relates more to the usefulness of the data in the progress of crack front regression. As such a large amount of hits is required to perform decent regression. Additionally the bias must be kept to a minimum by accurately knowing the receiver geometry and the speed of sound. Finally adhering to the SNR presented with the third research question is not only implied, but also explicitly stated.

12

Discussion

The conclusion presented in the previous chapter stated that this thesis was a work of learning. And I, now that I may use I, may say that it was the primary goal of this thesis. As long as I am a student the learning curve I go through trumps the explicitly stated goal that solves the problem I was presented with. So to correctly assess the quality of this thesis it is important to look at the process and progress in relation to myself, as a student rather than a researcher.

If I reflect upon the work I have done I need to look back slightly more than a year. This is a long period of time for a thesis. In this case it would be easy to dismiss the whole delay as resulting from the planning difficulties faced in relation to the experiments of the 4D-Fatigue JIP. However this dismissal would lack any form of self critique. And I may certainly criticise myself for the way in which I dealt with the difficulties faced.

It took me half a year of experimental failures before I sounded the alarm. My positive nature and curiosity assumed it would be all right in the end, and that the results would eventually come. This caused me to lose track of the planning, which led to a delay of four months. In case I came into action earlier I may have been able to mitigate the damage and graduate some months earlier.

Another reason for not noticing the problems with the planning and the delays earlier may be the means by which I communicated with my supervisors. With my supervisors at Vallen I mainly discussed technical details regarding acoustic emission and the processing methods. With my professor I discussed all kind of things, but often did not concern with the planning. In case I brought it up more, I may have been reminded that the current progress was not working towards the goal.

The advantage of a lot of critique is that it clearly states where the difficulties lie. As such I can use this information to improve upon myself. One learns best by making mistakes was the opening sentence of chapter 7, and now I know exactly how to improve. So I have learned.

Something about which I am satisfied is the ease by which the scope was altered. After noticing that the current progress was leading nowhere a quick decision was made to alter the scope and head to the office of Vallen Systeme for a sort of crisis session. The whole process including the stay with Vallen took just a few weeks. This showed resilience, which is a desired quality in research.

Additionally this project got me enthusiastic to continue in research, which may also be a reason why I did not feel the need to hurry up. The time that opened up as a result of the failing experiments has been used to define a new research project. In the end this new project instigated the feeling of urgency to finish, since the starting date of it was drawing near.

Regarding the contents of the thesis I have already mentioned that I wished I could have done more. Though in the end not all was possible. Some of the ideas that still roam my mind are presented in the next chapter as recommendations for further research.

13

Recommendations

Through this thesis the author aspired to reach the goal to the best of his ability. However, not everything could be covered. This chapter lists some of the suggestions for further research, which aims to further improve the quality of the acoustic emission fatigue crack monitoring system.

Regression Function. A regression function must be developed to translate the located source data into a crack front geometry. Such a function will construct the most likely crack front from the cloud of localised sources. Important questions to answer regarding such a regression model relate to the manner of dealing with an incrementing sample size, with sources originating from the crack surfaces, and to the manner by which the regression function operates.

Receiver Positioning & Speed of Sound. The receiver positioning algorithm presented in the exploratory work performs decently when it receives data of good quality, however, when it receives low quality data the error will stack incrementally for each newly localised receiver. Therefore an alternative is proposed, though not yet developed.

The basis of this new scheme should be geometry optimisation rather than geometry determination. The proposed principle is to establish a relation between the receivers by means of pulsing the channels. At the start rough definition of the receiver geometry and the speed of sound are used as input. This input will be used to localise the pulsed channels, possibly from time picked pulses. Localisation for each channel is bound to the surface of the specimen by means of planar localisation. A new speed of sound is determined from the localised receiver and recorded receiver pulse data. The new speed of sound and receiver locations are put back into the system for iterative improvement, until a satisfactory solution is obtained. This satisfactory solution will contain receiver positions and a speed of sound.

Alternatives to Time Picking. With the analysis of the state of the are novel time picking methods were evaluated. For the current study time-frequency domain onset detection was deemed to be to recourse intensive. However in other cases, or due to the improvement of processors, it may be of value. Therefore the quality of time-frequency domain time pickers should be investigated.

Planar Localisation. Planar localisation has been developed as a means to improve the quality of the results for the bar specimen, where the crack initiates outside of the receiver grid. It describes all volumetric localisation problems where the solution is reduced to a plane in that space. One coordinate in this solution is typically a function of the other two. In situations where the crack front has a continuous curvature this method of localisation may greatly improve the quality of the result. A prerequisite to the method is that the crack front is known, and may be described as a function. As such it is suitable for post-processing of data. In order to assess the assumptions on the quality improvement planar localisation should be studied more extensively.

Bibliography

[1] H. Akaike. Information Theory and an Extension of the Maximum Likelihood Principle. *2nd International Symposium on Information Theory*, pages 267–281, 1973.

[2] R. Allen. Automatic Phase Pickers: Their Present Use and Future Prospects. *Bulletin of the Seismological Society of America*, 72:225–242, 1982.

[3] F. Bai, D. Gagar, P. Foote, and Y. Zhao. Comparison of Alternatives to Amplitude Thresholding for Onset Detection of Acoustic Emission Signals. *Mechanical Systems and Signal Processing*, 84:717–730, 2017.

[4] L. de Broglie. A Tentative Theory of Light Quanta. *Philosophical Magazine*, 47-6:446–458, 1924.

[5] E.R. Fitzgerald. Particle Waves and Phonon Fission in Crystals. *Physics Letters*, 10-1:42–43, 1964.

[6] American Society for Nondestructive Testing. *Nondestructive Testing Handbook: Volume 5: Acoustic Emission Testing*. American Society for Nondestructive Testing, 2nd edition, 1987.

[7] C.U. Grosse and M. Ohtsu. *Acoustic Emission Testing: Basics for Research – Applications in Civil Engineering*. Springer-Verlag Berlin Heidelberg, 1st edition, 2008.

[8] D.V. Hinkley. Inference about the Change-Point from Cumulative Sum Tests. *Biometrika*, 58:509–523, 1971.

[9] J.T. Isaacs, D.J. Klein, and J.P. Hespanha. Optimal Sensor Placement For Time Difference of Arrival Localization. *Proceedings of the 48th IEEE Conference on Decision and Control*, 2009.

[10] ISO. ISO 5725-1: Accuracy (Trueness and Precision) of Measurement Methods and Results – Part 1: General Principles and Definitions, 1994.

[11] J. Kaiser. A Study of Acoustic Phenomena in Tensile Tests. Dr.-Ing. Dissertation, Technical University of Munich, 1950.

[12] J.D. Landstreet. Physical Processes in the Solar System, August 2003. http://www.astro.uwo.ca/~jlandstr/planets/webfigs/earth/images/waves.gif.

[13] A. Lee, S.F. Botten, E. VanDerHorn, and G. Wang. Structural Health Monitoring on Mooring Chain Using Acoustic Emission Testing. *Proceedings of the PRADS*, 2013.

[14] Granta Design Limited. CES Edupack 2016. 2016.

[15] N. Maeda. A Method for Reading and Checking Phase Times in Auto-Processing Systems of Seismic Wave Data. *Zisin / Jishin*, 38:365–379, 1985.

[16] R. Marks, A. Clarke, C. Featherston, C. Paget, and R. Pullin. Lamb Wave Interaction with Adhesively Bonded Stiffeners and Disbonds Using 3D Vibrometry. *Applied Sciences*, 6-1:12–41, 2016.

[17] A. Martin and M. Kortmann. mksqlite: A MATLAB Mex-DLL to SQLite Databases, April 2016. https://sourceforge.net/projects/mksqlite/.

[18] P.L. Nguyen, J. Vantomme, and D.G. Aggelis. Acoustic Emission Monitoring of Reinforcing Bars Pull-Out from Concrete Matrix. *World Conference on Non-Destructive Testing*, 19, 2016.

[19] D.C. Pack, W.M. Evans, and H.J. James. The Propagation of Shock Waves in Steel and Lead. *The Proceedings of the Physical Society*, 60-I(337), 1948.

[20] P.L. Pahlavan, J. Paulissen, R. Pijpers, H. Hakkesteeg, and R. Jansen. Acoustic Emission Health Monitoring of Steel Bridges. *European Workshop on Structural Health Monitoring*, 7:49–62, 2014.

[21] L.M. Rogers. Structural and Engineering Monitoring by Acoustic Emission Methods: Fundamentals and Applications. Technical Investigation Department, Lloyd's Register, 2001.

[22] A.A. Ronde, D.P. Dobson, P.G. Mededith, and S.A. Boon. Three-Dimensional Location and Waveform Analysis of Microseismicity in Multi-Anvil Experiments. *Geophysical Journal International*, 171:1282–1294, 2007.

[23] B. Scheeren. On the Validation and Preparation of Acoustic Emission Methods for Fatigue Analysis. Internship Report: Vallen Systeme GmbH & Delft University of Technology, September 2015.

[24] J. Schijve. *Fatigue of Structures and Materials*. Springer Netherlands, 2nd edition, 2009.

[25] B.H. Schofield. Acoustic Emission Under Applied Stress. Report ARL-150, Lessels and Associates, Boston, 1961.

[26] P. Sedlak, Y. Hirose, M. Enoki, and J. Sikula. Arrival Time Detection in Thin Multilayer Plates on the basis of Akaike Information Criterion. *Journal of Acoustic Emission*, 26:182–188, 2008.

[27] R. Sleeman and T. van Eck. Robust Automatic P-Phase Picking: an On-Line Implementation in the Analysis of Broadband Seismogram Recordings. *Physics of the Earth and Planetary Interiors*, 113:265–275, 1999.

[28] C.M. Sonsino and M. Kueppers. Multiaxial Fatigue of Welded Joints Under Constant and Variable Amplitude Loadings. *Fatigue & Fracture of Engineering Materials & Structures*, 24:309–324, 2001.

[29] C. Steffes. Field Experiments for TDoA-based Localization of GSM Base Stations. *Sensor Data Fusion: Trends, Solutions, Applications*, 2014.

[30] T. Thenikl, D. Altmann, and H. Vallen. Quantifying Location Errors. *32nd European Conference on Acoustic Emission Testing*, pages 495–502, 2016.

[31] Vallen Systeme GmbH. AMSY-6 System Description, April 2015.

[32] Vallen Systeme GmbH. Acoustic Emission Preamplifiers – Specification, April 2017.

[33] Vallen Systeme GmbH. Acoustic Emission Sensors – Specification, April 2017.

[34] Wikimedia Commons. Rayleigh Wave, March 2007.
https://commons.wikimedia.org/wiki/File:Rayleigh_wave.jpg.

[35] Wikimedia Commons. Accuracy: Trueness and Precision, April 2013.
https://commons.wikimedia.org/wiki/File:Accuracy_(trueness_and_precision).svg.

[36] J. Wong, L. Han, J.C. Bancroft, and R.R. Stewart. Automatic Time-Picking of First Arrivals on Noisy Microseismic Data. CREWES Research Report, University of Calgary, 2009.

A

The Relations Between Variance, Bias and Mean Squared Error

This appendix serves as an annotation with the definitions of precision, trueness and accuracy. It covers these topics in a mathematical sense by showing the relations between the variance, a measure of the precision, the bias, a measure of the trueness, and the mean squared error, a measure of the accuracy.

To start off this vivification the mathematical definitions of the accuracy measurements need to be understood. For these definitions $\hat{\theta}$ is used as an estimator of an unknown parameter θ. The following equation defines the variance:

$$\mathrm{Var}_\theta\left(\hat{\theta}\right) = \mathrm{E}_\theta\left[\left(\hat{\theta} - \mathrm{E}_\theta\left[\hat{\theta}\right]\right)^2\right] \tag{A.1}$$

This equation shows that the variance is the expected value of the squared difference between the estimator and the expected value of the estimator.

The bias is defined by the following equation:

$$\mathrm{Bias}_\theta\left(\hat{\theta}, \theta\right) = \mathrm{E}_\theta\left[\hat{\theta}\right] - \theta \tag{A.2}$$

This shows the bias to be the difference between the expected value of the estimator and the unknown parameter.

Finally the mean squared error is defined by:

$$\mathrm{MSE}\left(\hat{\theta}\right) = \mathrm{E}_\theta\left[\left(\hat{\theta} - \theta\right)^2\right] \tag{A.3}$$

Which shows that it is the expected value of the squared difference between the estimator and the unknown parameter.

The crux of this appendix is finding the binding fabric between these three accuracy concepts. To achieve this the mean squared error is used as a starting point.

$$\mathrm{MSE}\left(\hat{\theta}\right) = \mathrm{E}_\theta\left[\left(\hat{\theta} - \mathrm{E}_\theta\left[\hat{\theta}\right] + \mathrm{E}_\theta\left[\hat{\theta}\right] - \theta\right)^2\right] \tag{A.4}$$

On the right hand side equation the squared expression in between the brackets displays two distinct parts on either side of the plus-sign. The left part shows some resemblance to the definition of the variance, the right part to that of the bias.

It is key to isolate these parts. To that purpose the squared expression is expanded to:

$$\mathrm{MSE}\left(\hat{\theta}\right) = \mathrm{E}_\theta\left[\left(\hat{\theta} - \mathrm{E}_\theta\left[\hat{\theta}\right]\right)^2 + 2\left(\hat{\theta} - \mathrm{E}_\theta\left[\hat{\theta}\right]\right)\left(\mathrm{E}_\theta\left[\hat{\theta}\right] - \theta\right) + \left(\mathrm{E}_\theta\left[\hat{\theta}\right] - \theta\right)^2\right] \tag{A.5}$$

In this equation three parts separated by plus-signs are visible. These include the left and right parts that have previously been identified as resembling the respective variance and bias.

Knowing that the expected value of a sum is equal to the sum of the expected values, i.e. linearity, allows the following isolation of terms:

$$\mathrm{MSE}\left(\hat{\theta}\right) = \mathrm{E}_\theta\left[\left(\hat{\theta} - \mathrm{E}_\theta\left[\hat{\theta}\right]\right)^2\right] + \mathrm{E}_\theta\left[2\left(\hat{\theta} - \mathrm{E}_\theta\left[\hat{\theta}\right]\right)\left(\mathrm{E}_\theta\left[\hat{\theta}\right] - \theta\right)\right] + \mathrm{E}_\theta\left[\left(\mathrm{E}_\theta\left[\hat{\theta}\right] - \theta\right)^2\right] \tag{A.6}$$

This expression shows the same three parts on the right hand side of the equation, though now as isolated expected values. Clearly visible is the variance in the leftmost part of the right hand side.

The next step is to identify that $\left(\mathrm{E}_\theta\left[\hat{\theta}\right] - \theta\right)$ is a constant, and to know that the expected value of a constant is equal to that constant. This reduces equation A.6 to:

$$\mathrm{MSE}\left(\hat{\theta}\right) = \mathrm{E}_\theta\left[\left(\hat{\theta} - \mathrm{E}_\theta\left[\hat{\theta}\right]\right)^2\right] + 2\mathrm{E}_\theta\left[\hat{\theta} - \mathrm{E}_\theta\left[\hat{\theta}\right]\right]\left(\mathrm{E}_\theta\left[\hat{\theta}\right] - \theta\right) + \left(\mathrm{E}_\theta\left[\hat{\theta}\right] - \theta\right)^2 \tag{A.7}$$

This equation shows that the rightmost part of the right hand side is the bias squared. This bias is also visible in the central part, where it is multiplied by $2\mathrm{E}_\theta\left[\hat{\theta} - \mathrm{E}_\theta\left[\hat{\theta}\right]\right]$.

The expected value in this multiplication can be expanded by knowing that the expected value of the estimator is a constant; as such it reduces to $2\left(\mathrm{E}_\theta\left[\hat{\theta}\right] - \mathrm{E}_\theta\left[\hat{\theta}\right]\right)$. Substituting this into equation A.7 gives:

$$\mathrm{MSE}\left(\hat{\theta}\right) = \mathrm{E}_\theta\left[\left(\hat{\theta} - \mathrm{E}_\theta\left[\hat{\theta}\right]\right)^2\right] + 2\left(\mathrm{E}_\theta\left[\hat{\theta}\right] - \mathrm{E}_\theta\left[\hat{\theta}\right]\right)\left(\mathrm{E}_\theta\left[\hat{\theta}\right] - \theta\right) + \left(\mathrm{E}_\theta\left[\hat{\theta}\right] - \theta\right)^2 \tag{A.8}$$

This shows that the bias in the central part of the right hand side is multiplied by two times zero.

This means that equation A.8 can be reduced to the following:

$$\mathrm{MSE}\left(\hat{\theta}\right) = \mathrm{E}_\theta\left[\left(\hat{\theta} - \mathrm{E}_\theta\left[\hat{\theta}\right]\right)^2\right] + \left(\mathrm{E}_\theta\left[\hat{\theta}\right] - \theta\right)^2 \tag{A.9}$$

This equation only leaves the final step of identifying the variance and the squared bias as the result of the derivation.

As such the relation between the three accuracy concepts is as follows:

$$\mathrm{MSE}\left(\hat{\theta}\right) = \mathrm{Var}_\theta\left(\hat{\theta}\right) + \mathrm{Bias}_\theta\left(\hat{\theta}, \theta\right)^2 \tag{A.10}$$

B

Time Picking Relevance and Functions

The contents of this appendix have been taken from the exploratory work performed by Scheeren [23].

Time picking is the process of selecting the time of arrival of a transient wave. As mentioned earlier it is common practice to determine the TOA by a threshold crossing. Though this method is widely applied it is a very crude one. Figure B.1 shows how small differences in a signal can lead to significantly different time picks. The figure shows a single event which has been sampled by receivers on five locations. The blue lines display a time trace of the transient recording, the red lines display the threshold picked arrival times on each of these time traces. All signals have been shifted manually so that the S_0 arrival is synchronized. Ideally all red lines should match up vertically, since this would indicate that the same part of the wave is picked for each of the cases. This however is not the case.

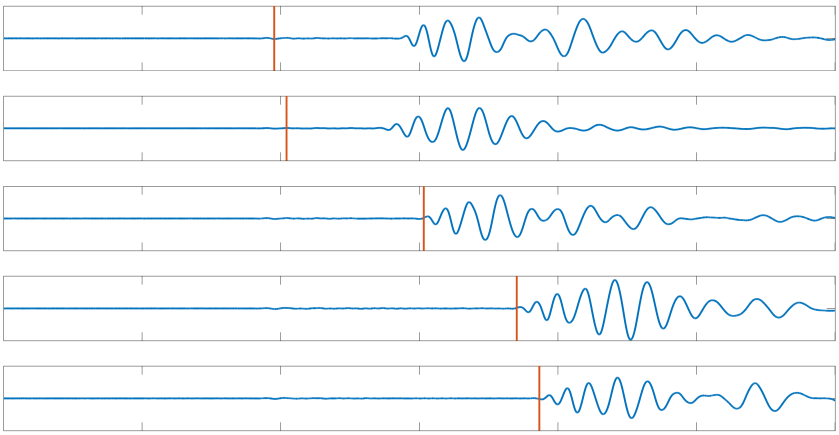

Figure B.1: Threshold Picking Alteration of Five Channel Acoustic Event

Two types of threshold picking errors are identified. The first is the "S_0-A_0 alteration", which describes bad picks due to wave mode inconsistency. Depending on the threshold settings and small differences in the emission strength threshold time picks may alternate between the S_0 arrival time and the A_0 arrival time. This picking error often accounts for large errors in TDOA. This type of alteration is clearly shown by comparing the top two signals with the bottom three signals of figure B.1.

With this type of alteration it should also be noted that each wave mode travels at its own velocity. Therefore this type of alteration leads to a bigger error the further the receivers are from the event. Regarding the consistent detection of either S_0 or A_0 for localisation there is no preference, however the A_0 wave is of larger magnitude and thus easier to detect.

The second type of error is the "near miss near hit alteration". This describes bad picks resulting from inconsistency in a near miss or a near hit of a specific half wave. It typically leads to a picking error in the order of half a wave period to a single wave period, which accounts for 3 μs to 7 μs. This type of alteration is clearly shown in the top two signals of figure B.1.

In order to improve upon these errors several time picking schemes are proposed and evaluated. Each of these time picking schemes evaluates the sampled transient waveform in an attempt to detect amplitude, frequency and or phase change. Samples in the transient recordings are indicated by U_n with $n \in \{1 : N\}$. To give some idea of the sensitivity of the time picking functions they are all applied to the sample wave shown in figure B.2.

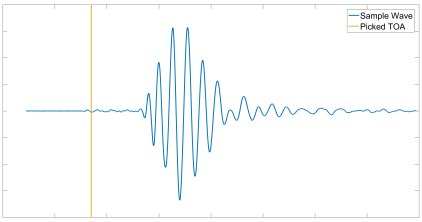

Figure B.2: Threshold Picked Acoustic Wave

Maximum Amplitude. A very simple scheme to substitute for the threshold picked arrival times is the Maximum Amplitude (MA) picker. As the name suggests it picks the TOA at the absolute maximum sample of the recorded transient wave.

The expectancy is that this method, compared to the threshold based TOA, will result in a more consistent TOA. The main reasons for this is that it suffers from neither the "S_0 A_0 alterations" nor the "near miss near hit alterations". The maximum amplitude pick of the sample wave is shown in figure B.3.

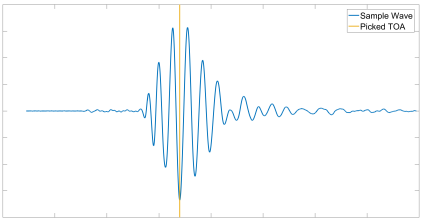

Figure B.3: MA Picked Acoustic Wave

Short Term Average Long Term Average. Another relatively basic method of detecting changes in a signal is the evaluation of the Short Term Average Long Term Average (STALTA). This method compares the averages over two time windows to observe local changes from the global trend. The STALTA function is given by:

$$\text{STALTA}_n = \frac{\frac{1}{W_{ST}} \sum_{m=n-W_{ST}}^{n} U_m^2}{\frac{1}{W_{LT}} \sum_{m=n-W_{LT}}^{n} U_m^2} \tag{B.1}$$

In this equation W_{ST} and W_{LT} refer to the length of the respective short term and long term time windows. For the analysis of transient waves these parameters have to be carefully tuned. Currently the short term window is set to a length of 5 μs and the long term window is set to 50 μs, though these values have not been fine-tuned to obtain the best pick.

The TOA is picked from the STALTA function at the maximum positive difference given by:

$$\delta_{\text{STALTA}_n} = \text{STALTA}_{n+1} - \text{STALTA}_n \tag{B.2}$$

This difference function has been plotted against the sample wave in figure B.4. This figure shows a somewhat fluctuating function. This is an undesired feature since it does not favour only a single point in time. A second undesired feature is the selection of time windows. Slight variations in these windows might alter the time pick.

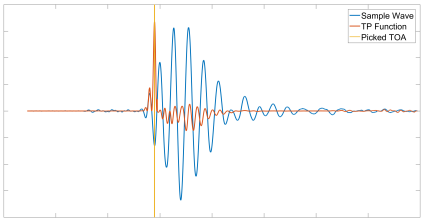

Figure B.4: STALTA Picked Acoustic Wave

Energy Ratio. Very similar to the STALTA picker is the Energy Ratio (ER) picker. It also compares the energy of two moving windows to each other, the difference with STALTA being that both windows are of the same size and that the windows are positioned both left and right of the evaluated sample. The ER function is given by:

$$\mathrm{ER}_n = \frac{\sum_{m=n-W_{ER}}^{n} U_m^2}{\sum_{m=n}^{n+W_{ER}} U_m^2} \tag{B.3}$$

Here W_{ER} indicates the length of the energy ratio time window, which has been set to 5 μs. An optimization of the time picking scheme may be possible by fine-tuning the time window. For now the window of 5 μs has been used, which resulted in figure B.5 when applied to the sample wave.

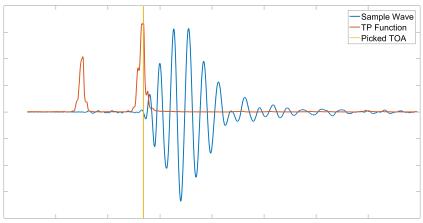

Figure B.5: ER Picked Acoustic Wave

This method identifies both wave mode arrivals, though the peaks at each arrival seem somewhat vaguely formed. This could be the result of window optimization, though as stated before; methods that depend greatly on a specific window are undesired.

An alteration to the energy ratio picker is the Modified Energy Ratio (MER) picker [36]. The function of the MER is given by:

$$\mathrm{MER}_n = |U_n|\mathrm{ER}_n^3 \tag{B.4}$$

Where $|\ldots|$ indicates the absolute value. This modification reduces the sensitivity to small changes in the signal. This is also clearly shown in figure B.6. Unlike the ER function displayed in figure B.5 this function is only sensitive to the strongest wave mode arrival. However the arrival itself is still characterized by a somewhat vague broad peak. This might lead to inaccuracy.

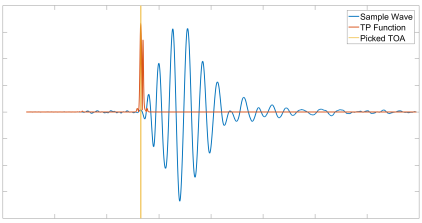

Figure B.6: MER Picked Acoustic Wave

Hinkley Criterion. Another time picker that evaluates the energy of the wave is the Hinkley Criterion (HC) picker. It is based on the work of Hinkley [8]. It compares the sum of the energy up to a certain point in time with the expected value of that energy based on a linear estimation. The time picking function of the Hinkley Criterion is defined as:

$$\mathrm{HC}_n = \sum_{m=1}^{n} U_m^2 - \frac{n \sum_{m=1}^{N} U_m^2}{\alpha N} \tag{B.5}$$

In this equation α is a parameter to scale the subtractive trend. It is a means of slightly shifting the minimum. For the purpose of this report only $\alpha = 1$ has been considered.

Applied to the sample wave the HC picker results in the graph of figure B.7. This function shows only a single clear minimum which is present on the A_0 arrival. The point it picks lies somewhere on the wave, and not at the actual onset. Though this will not be an issue, as long as it consistently picks the same point on each wave.

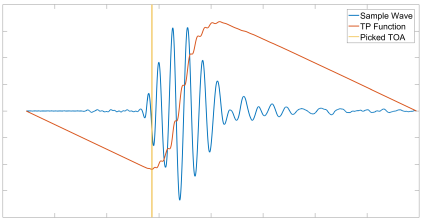

Figure B.7: HC Picked Acoustic Wave

Akaike Information Criterion. A different means of looking at changes in the signal is by evaluating the variance. This is what the Akaike Information Criterion (AIC) picker does. It is based on the work of Akaike in information theory [1]. The AIC function applicable for acoustic emission signals is an adaption of Akaike by Maeda for the purpose of seismological research [15, 22]. It is defined as:

$$\mathrm{AIC}_n = n \log_{10}(\mathrm{Var}[U_{n-}]) + (N - n - 1)\log_{10}(\mathrm{Var}[U_{n+}]) \tag{B.6}$$

Here $n-$ indicates all samples before and including n (i.e. $[1:n]$), and $n+$ indicates all samples after and excluding n (i.e. $[n+1:N]$). Applying this function to the sample wave returns figure B.8.

Similar to the HC function the AIC function seems to show a downward trend. The minimum of the function indicates the onset. There are some more interesting observations. Most notably is the significantly pronounced local minimum before the actual picked onset. This minimum indicates the onset of the S_0 wave. The selection of the A_0 onset as the main onset is the result of a much more pronounced variance change there between S_0 and A_0. It may be imaginable that for some waves the clear difference between these two arrivals is not as present. This might result in "S_0-A_0 alteration", though errors could be identified and removed by further (auto)analysing the time picking function. There have also been investigations into multi-stage AIC pickers that could improve accuracy [26].

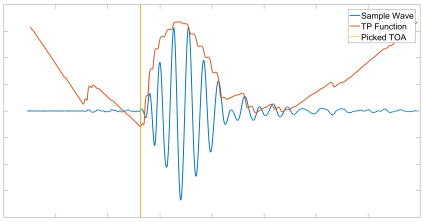

Figure B.8: AIC Picked Acoustic Wave

Baer & Kradolfer. A somewhat more complex time picking function has been designed by Baer and Kradolfer [27]. In this report it is referred to as the Baer & Kradolfer (BK) picker. It uses an elaborate envelope function that is based on the work of Allen [2], which is given by:

$$e_n^2 = U_n^2 + \dot{U}_n^2 \frac{\sum_{m=1}^{n} U_m^2}{\sum_{m=1}^{n} \dot{U}_m^2} \tag{B.7}$$

The evaluation of the derivative ($\dot{U}$) in the BK envelope function (e) is done by an upwind scheme that does not take the sampling rate into account ($\dot{U} = \delta_U$ as in eq. B.2). A result of this derivative is that the samples in the envelope are limited to $n \in \{1 : N-1\}$.

From this envelope the BK function is calculated as:

$$\mathrm{BK}_n = \frac{e_n^4 - \overline{e_{n-}^4}}{\mathrm{Var}\,[e_{n-}]} \tag{B.8}$$

Where $n-$ indicates all samples before and including n (i.e. $[1:n]$), $\mathrm{Var}\,[\ldots]$ denotes the variance, and $\overline{\ldots}$ denotes the mean. Evaluation of the sample wave using the BK picker results in the graphs presented in figure B.9. Visible in the graph is a function that has a very distinct peak close to the arrival of the A_0 wave mode. This seems to indicate consistency of the picker.

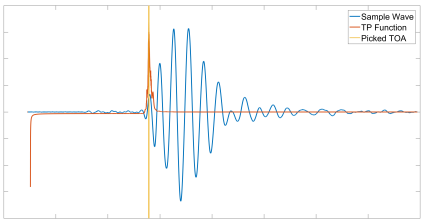

Figure B.9: BK Picked Acoustic Wave

C

Bar Specimen

Initially experimental research into the monitoring of fatigue cracks was the principle task in the scope of work. However, due tot he lack of results this task was removed from the main matter of the thesis. This appendix covers a guide to the bar specimen experiments, and presents and discusses the insights gained from these experiments.

At first this appendix covers the geometry of the bar specimen. Following on this it presents the methods for data acquisition, which elaborate on receiver configurations, and the methods for data processing are discussed, which further illustrate the localisation problem faced with the bar specimen and presents the solution to this problem. Finally the results from three experiments are presented and discussed.

C.1. Specimen Geometry

The considered bar specimen is a variant of the hourglass specimen. It has a cylindrical attachment at the longitudinal centre, where a typical hourglass specimen has the lowest cross sectional area. The whole specimen is turned from a single piece of shaft steel (S355J2G3). Figure C.1 displays a isometric projection of the custom bar specimen. Figure C.2 displays a side projection of half of the bar specimen including the considered reference frame. L denotes the longitudinal direction and T the transverse direction, both are perpendicular to each other. A third reference direction is the angle θ_T. The zero point of this angle is somewhat arbitrary, though is defined to be in the direction of receiver one (R_1).

The design of the specimen is intended to simulate an infinite double sided transverse attachment. In this description infinite refers to the simulated weld length, it is continuous; i.e. without a beginning or an end. Double sided refers to the tapered connection between the attachment and the bar, the simulated weld, which is present on both sides of the attachment.

When subjected to repeated uni-axial loading the specimen is intended to accumulate fatigue damage and eventually fracture. The location for this damage accumulation is, in the first experiments, unknown due to the intact geometry and lack of imperfections. What is known is that the crack will initiate from a hot-spot, where the stress is highest. This hot-spot occurs at the weld toe, the point where the simulated weld meets the bar. From this initiation point the crack is expected to grow in through-thickness direction.

In later experiments an initial defect is introduced with the intention of bypassing the crack initiation period. This makes the origin of the fatigue crack known, allowing for a more specific receiver geometry.

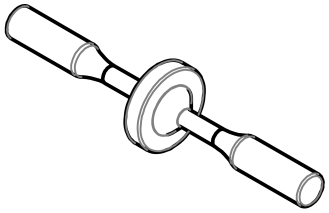

Figure C.1: Isometric Projection of Bar Specimen

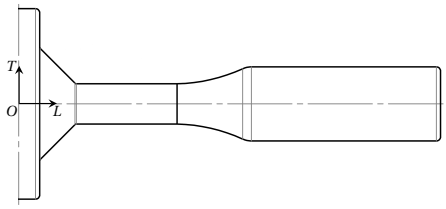

Figure C.2: Side View of Bar Specimen Including L–T Reference Frame

C.2. Methods for Data Acquisition & Processing

Three bar specimen of the 4D-Fatigue JIP have been instrumented with acoustic emission hardware and tested in an Instron E10000 bi-axial tension-torsion testing machine. This section elaborates on the methods used for recording and processing data from these instrumented specimen.

In general the recording procedure for a measurement campaign composes of three parts. Prior to starting the experiment the operability of the acoustic emission measurement system is validated. This measurement is performed in hit-based[1] recording mode. The main purpose of this step is to validate the coupling of each of the receivers to the specimen. The coupling is validated using both pencil lead breaks and receiver pulsing.

For the second step the measurement system is switched to continuous[2] recording mode. For the next 15 minutes the initialisation of the test and the background noise are recorded. This measurement is used to fine-tune the detection threshold for the actual measurement.

The final part of the recording procedure covers data collection over the course of the fatigue test. This is performed in hit-based recording mode. Over the course of the test markers will be added to the data to record the number of cycles and visual observations.

Planar Localisation The geometry of the bar specimen complexifies event localisation. Due to the presence of the attachment and the absence of a hollow geometry receivers can only be situated closely to the notch on one side of the fracture plane. As such volumetric localisation is impaired. Planar localisation is proposed to accommodate for this by reducing the solution space of the localisation problem.

The basis of planar localisation is governed by the assumption that the crack will only develop through a plane which may be captured by a continuous mathematical expression. This plane through which the crack is assumed to propagate will be denoted as the source plane, or alternatively the fracture plane (figure C.3). A local reference system is used to define the source plane and the receiver coordinates. This local system is a transformation of the global system, which is shown in figure C.2, where the origin is shifted along L to coincide with the centre of the cross section at the simulated weld toe. In this transformation T and θ_T remain unchanged. The local system is denoted by $L'T\theta_T$.

The receiver coordinates and fracture plane will be specified relative to this local system. The post-processing system operates in a Cartesian (XYZ) coordinate system. Transformation from the $L'T\theta_T$-system to the XYZ-system is performed in accordance with the following equations:

$$X = T\cos(\theta_T) \tag{C.1}$$

$$Y = T\sin(\theta_T) \tag{C.2}$$

$$Z = L' \tag{C.3}$$

For planar localisation a reduced version of LUCY is solved using a black-box multi-variable non-linear minimisation function. In this reduced version the z-coordinate of the solution is imposed to be a function of x and y ($z = f(x,y)$). This function describes the mathematically captured fracture plane. A result of this substitution of the z-coordinate is that it limits the solution space of the estimated range difference, reducing the LUCY to a two-dimensional problem.

However, before planar localisation can be applied it must first be validated with respect to accuracy. There are two parameters that influence the accuracy of planar localisation. Both of these relate to receiver placement relative to the fracture plane, figure C.3 provides a further illustration with this. The first influencing parameter is the alignment of the receiver and the fracture plane. The best localisation results are most likely obtained when the receiver and source plane are parallel. However, this requires a-priori knowledge on the shape of the crack, which is typically unavailable. The best alternative to suit all crack planes is most likely a receiver plane perpendicular to the L'-direction as shown in figure C.3. The second influencing parameter relates to the offset of the receivers in comparison to the fracture plane. In this case the closest approach will provide the best accuracy. However in practice the specimen and receiver geometry dictate a certain offset. It is crucial to assess the influences of these to parameters on the accuracy of planar localisation in order to validate the use of planar localisation.

[1] Data acquisition based on time slices around threshold crosses.
[2] Data acquisition based on continuous time slices.

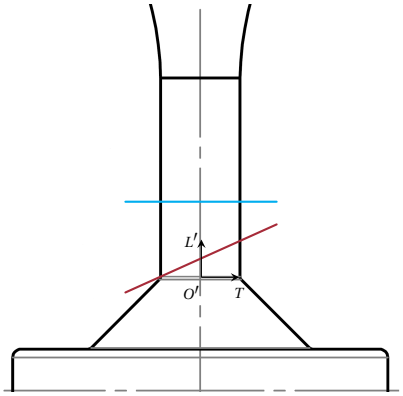

Figure C.3: Receiver-Fracture Offset – Side View
Depiction of the distance between the receiver plane (blue) and the fracture plane (red)

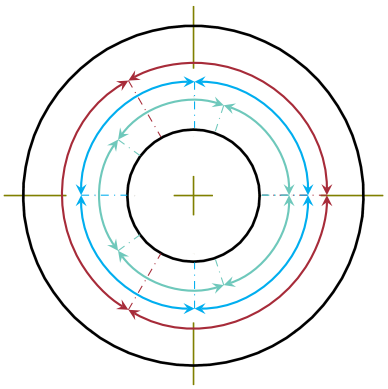

Figure C.4: Bar Specimen Receiver Array – Top View
Depiction of angular placement of three receiver array (red), four receiver array (blue) and five receiver array (green)

Receiver Geometry Considering the assumptions made for planar localisation only a few options remain to instrument the specimen. As was stated when the concerns with with planar localisation were mentioned a receiver plane perpendicular to the L'-direction is the best option in case detailed a-priori knowledge on the shape of the fracture plane is unavailable. This receiver plane is also depicted in figure C.3 by the blue line.

The placement of a specific number of receivers in the plane is restricted to either a free-form or a regularly spaced array. Regarding planar array optimisation Isaacs et alii have shown that the optimal array is regularly spaced and symmetric [9]. This leaves only the number of receivers to be selected, which relates to the accuracy and redundancy of the array. Figure C.4 shows three regularly spaced receiver arrays composed three through five receivers. Three receivers are the absolute minimum to localise sources in plane, though this provides no redundancy for a bad recording. Five receivers provides some redundancy and thus more robust localisation.

Bar-3 Bar-3 was the first specimen on which acoustic emission measurement has been applied. The intent of this measurement was to acquire a qualitative dataset by which acquisition parameters may be fine-tuned for further measurement campaigns. Localisation has not yet been aspired for this measurement. As such the specimen is instrumented with only four receivers. These receivers are placed on either side of the attachment, close to and further away from the notch. Since no localisation is aspired yet the exact positioning of these receivers is not critical. Figure C.5 displays a bar specimen with receivers in an Instron E10000 bi-axial tension-torsion testing machine. The receivers positions in this figure are representative for Bar-3.

Bar-5 Bar-5 was a second attempt to perform the Bar-3 measurement. As such all conditions but the load level are kept constant. For this experiment the load level is lowered. Figure C.5 displays the experimental set-up of Bar-5.

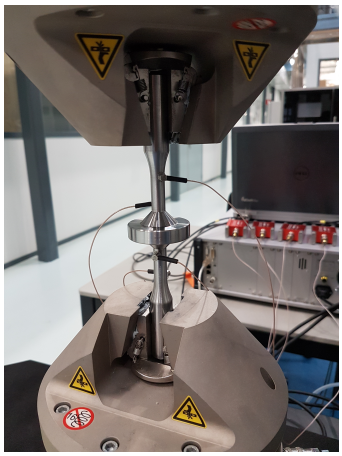

Figure C.5: Experimental Set-up of Bar-5

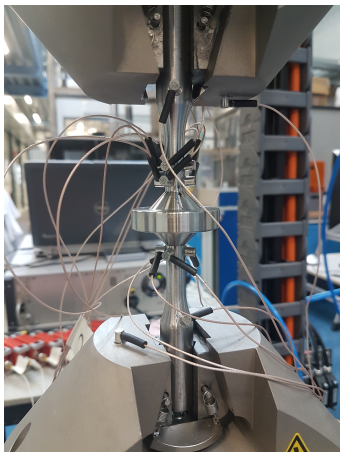

Figure C.6: Experimental Set-up of Bar-D100mum

Bar-D100mum For the third experiment a initial defect was introduced in the shape of an elliptical surface crack with a depth of 100 µm and a length of 400 µm. This specimen has been instrumented with a receiver grid suitable for localisation. Figure C.6 displays the specimen, with receivers, in the Instron E10000 bi-axial tension-torsion testing machine. The receiver grid composes of two receiver planes above the notch containing the defect, and a single receiver plane below the intact notch. Four more receivers are placed as guards on either the specimen or the clamps of the testing machine. All of the receivers around the notch are placed in accordance with the four receiver option shown in figure C.4. The radial positions of the three planes are all in line. Two receiver planes are applied on the side of the defect to improve accuracy and redundancy. The four guard receivers closer to, or on top of, the clamps are used to isolate signals coming from the testing machine.

C.3. Recorded Data

Three attempts have been made to record acoustic emissions generated by the fatigue fracturing of the specimen. Each of these attempts has been unsuccessful. Each of the specimen showed no visual signs of fatigue cracking after being classified as run-outs.

Bar-3 For the first of the bar specimen, instrumented for qualitative measurement, only a continuous recording has been made. During this recording it became clear that the specimen experienced significant plastic deformation. At a rotation of 90° the test was halted and deemed a failure due to plastic deformation. Because of this plastic deformation the acoustic emission data collected with this test was considered not to be representative for fatigue fracturing.

Bar-5 The second bar specimen has been tested following directly on the first one. Due to the lower load level it suffered less from plasticity, though some local plasticity around the notch was still observed. As a result of this plasticity the specimen deformed up to a rotation of about 45°, where it remained stable for the rest of the experiment. This stable position is also shown in figure C.5. Eventually the experiment was halted close to 10^7 cycles. It was classified a run-out. No visible signs of damage initiation were obtained. With respect to the collected acoustic emission data there was no activity which might show any indication of crack initiation.

Bar-D100mum After two failed attempts with intact geometries an initial defect was added in a notch of the specimen. This defect represented an elliptical surface crack with a depth of 100 µm and a length of 400 µm. This specimen has been tested in three stages. The first of these covered $7.2 \cdot 10^6$ cycles at a varying load up to 100 MPa in shear. During the experiment problems in the laboratory led to a shut-down and restart of the test twice. Recorded acoustic emission data and visual inspection of the specimen showed no signs of crack growth.

A month and a half later the same specimen was mounted in the testing apparatus again for a continuation of the earlier test. It has been subjected to another $3.9 \cdot 10^6$ cycles at a varying load up to 100 MPa in shear. No problems were faced during this test. At the end no indications, both acoustically or visibly, were present of any crack growth. At this time the specimen had been subjected to a total of $11.1 \cdot 10^6$ cycles at a varying load up to 100 MPa in shear.

In an attempt to obtain a fracture within reasonable time the same specimen was subjected to another test at a higher load level. For this test the cyclic load was increased to up to 150 MPa in shear. After another $5.0 \cdot 10^6$ cycles there were still no acoustic or visible signs of crack growth. The test was also deemed a run-out.

C.4. Discussion

In summary three bar specimen were instrumented with acoustic emission hardware and tested on an Instron E10000 bi-axial tension-torsion testing machine. None of the experiments led to fracture and thus no usable data to validate the ability of the post-processing system was obtained. This means that the data for validation of the system must be acquired through a different procedure. Another obstacle the missing data imposes is that there has been no possibility yet to validate planar localisation. This is also suggested to remain a task for further research.

D

Tubular Specimen

Initially experimental research into the monitoring of fatigue cracks was the principle task in the scope of work. However, due tot he lack of results this task was removed from the main matter of the thesis. This appendix covers a guide to the tubular specimen experiments, and presents and discusses the insights gained from these experiments.

At first this appendix covers the geometry of the tubular specimen. Following on this it presents the methods for data acquisition, which elaborate on receiver configurations. Finally the results from three experiments are presented and discussed.

D.1. Specimen Geometry

The considered tubular specimen is a hollow cylinder which contains two continuous circular attachments perpendicular to the longitudinal direction of the cylinder. Flanges at the ends of the tube serve as an interface to the testing apparatus. The whole specimen is turned from a single piece of shaft steel (S355J2G3). An isometric projection of the tubular specimen is depicted in figure D.1. A close-up of the cross-section around the attachments is displayed in figure D.2. The specimen has been designed with two attachments to investigate the possibility of simultaneous crack growth in a single specimen.

The design of the specimen is intended to simulate an infinite double sided transverse attachment. The weld geometry is simulated by the tapered connection between the attachment and the tube. Due to the cylindrical geometry the simulated weld is continuous and thus has infinite length. The tapered connection on both sides of the attachment simulates a double sided weld.

When subjected to repeated loading the specimen is intended to accumulate fatigue damage and eventually fracture. The origin for this damage accumulation is known, since initial defects are present in the notches of both of the attachments. These defects are shaped like an elliptical surface crack with a depth of 100 µm and a length of 400 µm. The defects are positioned as far as possible from each other to minimise the effect one of the cracks might have on the other. This means the cracks are positioned on opposite sides of the circumference of the tubular in the notches facing the flanges.

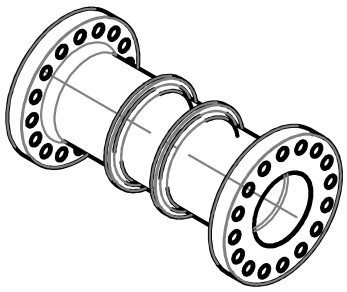

Figure D.1: Isometric Projection of Tubular Specimen

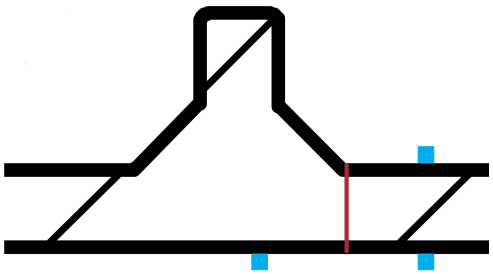

Figure D.2: Detail of Attachment on Tubular Specimen Including expected uni-axial tension fracture plane (red) and proposed receiver positions (blue)

D.2. Methods for Data Acquisition

A single tubular specimen of the 4D-Fatigue JIP has been instrumented with acoustic emission hardware and tested in a 1000 kN MTS fatigue testing machine. This section elaborates on the methods used for recording and processing data from this instrumented specimen.

In general the recording procedure for a measurement campaign composes of three parts. Prior to starting the experiment the operability of the acoustic emission measurement system is validated. This measurement is performed in hit-based[1] recording mode. The main purpose of this step is to validate the coupling of each of the receivers to the specimen. The coupling is validated using both pencil lead breaks and receiver pulsing.

For the second step the measurement system is switched to continuous[2] recording mode. For the next 15 minutes the initialisation of the test and the background noise are recorded. This measurement is used to fine-tune the detection threshold for the actual measurement.

The final part of the recording procedure covers data collection over the course of the fatigue test. This is performed in hit-based recording mode. Over the course of the test markers will be added to the data to record the number of cycles and visual observations.

Receiver Geometry The highest localisation accuracy can be obtained if the source of an acoustic event is situated within the boundaries of the receiver array. As such the receiver array should span a volume around the expected crack plane. For the case of uni-axial tension, to which the considered tubular specimen is subjected, the crack is expected to grow perpendicular to the loaded direction. This expected fracture plane is depicted in the cross-section of the attachment presented in figure D.2. This figure also displays the cross-section of the proposed receiver array. The cross section of this array composes of one receiver on the outside of the tube close to the attachment, and two receivers on the inside of the tube. At least two of these arrays must be placed at the far ends of the expected through-thickness crack in order to allow for localisation of the sources originating from the propagating crack front. Additional arrays along the length of the crack increase the accuracy and robustness of the localisation procedure.

The tubular specimen under consideration needs to be instrumented for two sources. Both of these will be enclosed in an array of six receivers. These six receivers have been positioned in two cross-sectional three receiver arrays as depicted in figure D.2. Additionally four receivers are placed as guards. Two of these guards are placed on opposite sides of the longitudinal centre of the specimen, and serve to isolate signals travelling from one defect to the receiver array around the other defect. The other two guards are placed close to the flanges to isolate signals coming from the testing machine.

Figure D.3: Experimental Set-up of Tubular Specimen

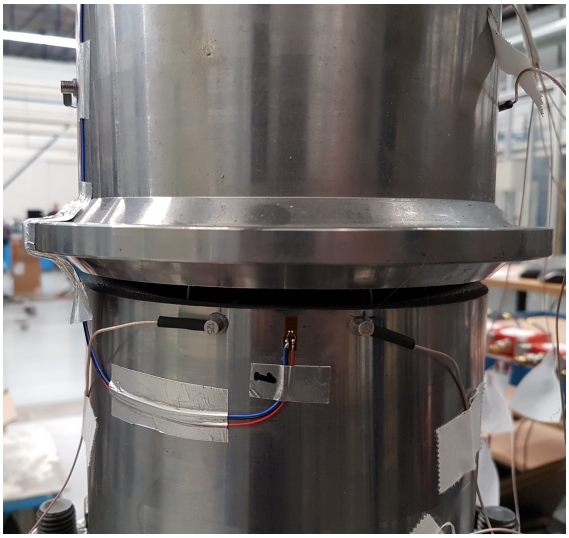

Figure D.4: Close-up of Fracture of Tubular Specimen

[1] Data acquisition based on time slices around threshold crosses.
[2] Data acquisition based on continuous time slices.

D.3. Recorded Data

A single measurement has been performed with an instrumented tubular specimen. Figure D.3 shows the instrumented tubular specimen in the 1000 kN MTS fatigue testing machine. The continuous measurement has shown that the background noise levels of the 1000 kN MTS fatigue testing machine exceed 80 dB_{AE}. Common practice in the acoustic emission industry is to break-off a test in case the background noise is higher than 70 dB_{AE}. Since this is a research application the measurement was continued in an attempt to record any usable data despite the high threshold.

After several days of testing the specimen fractured at one of the two defects, as depicted in figure D.4. Over the course of these days more than 200 gigabytes of data has been collected. A review of this data has shown most of it to originate from the testing machine. A few events originated from within the receiver array surrounding the fractured initial defect. However, these most of these events did not meet the requirements for the amount of hits needed for localisation, or contained hits which could not be time picked correctly due to the low signal to noise ratio. In summary no qualitative data was obtained on the crack propagation.

D.4. Discussion

The single test with the tubular specimen has shown that the 1000 kN MTS fatigue testing machine is unsuitable for acoustic emission research due to the high background noise. Further acoustic emission measurements on the tubular specimen are postponed until a fatigue testing apparatus with a better noise characteristic becomes available. In order to validate the post-processing stem another procedure must be defined to obtain volumetric source data.